

2021

Measuring the internal geometry of an anastomosed synthetic blood vessel under internal pressure

Grocock, Jay

Grocock, J. (2021) 'Measuring the internal geometry of an anastomosed synthetic blood vessel under internal pressure', *The Plymouth Student Scientist*, 14(1), pp. 206-245.

<http://hdl.handle.net/10026.1/17332>

The Plymouth Student Scientist

University of Plymouth

All content in PEARL is protected by copyright law. Author manuscripts are made available in accordance with publisher policies. Please cite only the published version using the details provided on the item record or document. In the absence of an open licence (e.g. Creative Commons), permissions for further reuse of content should be sought from the publisher or author.

Measuring the internal geometry of an anastomosed synthetic blood vessel under internal pressure

Jay Grocock

Project Advisor: [Adam Kyte](#), School of Engineering, Computing and mathematics, University of Plymouth, Drake Circus, Plymouth, PL4 8AA

Abstract

For this paper, a simple inexpensive rig system was designed and two methods for imaging and measuring how a synthetic representation of an anastomosed artery deforms under internal pressure were used. An optical method with a camera and a Computed Tomography (CT)-based imaging method were used. Cylindrical samples of Natural Rubber Latex were anastomosed and subject to extension-inflation tests to represent an artery under the physiological conditions of the body. The simple rig system was designed to apply physiological levels of internal pressure to the latex tubing. The two imaging methods were used to monitor variations in the circumferential and longitudinal extension as a function of the applied pressure. The CT scanner has the additional ability to view inside the specimen and give an understanding of how the tension in the sutures affects the internal and external shape of the specimen. The two methods, optical and CT, were compared to each other and to theoretical predictions to assess the potential limitations of each of these methods. Quantifying and understanding the material properties of the synthetic representation used proved to be an imperative part of the investigation to predict and understand how the specimen would deform. In conclusion, the CT measurements were likely to provide the most reliable results. Departures in the measurements from theoretical predictions means that empirical methods should continue to be applied to studies modelling anastomosed arteries and used to improve theoretical predictions.

Keywords: anastomosed synthetic blood vessel, internal geometry, computed tomography, modelling, theoretical predictions, synthetic representation.

Introduction

An anastomosis is the surgical procedure of connecting two adjacent conduit structures. This paper was concerned with the joining of arteries or veins (vascular anastomosis) with sutures (stitches). After 50 years of coronary artery bypass grafting, it still remains the most common cardiac surgery in the world with approximately 200,000 procedures annually in the US, highlighting the importance of these procedures (Melly et al., 2018). As well as cardiac surgery, common vascular surgery, trauma surgery, atherosclerosis (hardening and narrowing of arteries) and aneurysms (localised bulging or a weakened spot) often require surgical anastomosis and are common routine reconstruction procedures. For arterial reconstruction, the damaged regions are often removed and then either stitched back to a healthy artery or repaired through the insertion of a synthetic graft or autologous grafts (from the same patient). This technique is commonly known as end-to-end anastomosis (Roussis et al., 2015).

Unfortunately, even after successful surgery, restenosis and long-term graft failure are common. The long-term success of these surgeries is dependent on a number of factors. The addition of an anastomosis and sutures to the artery can play a role in creating “non-physiological flow dynamical and wall mechanical conditions” which lead to irregular conditions in the artery. This can include flow separation, mechanical wall stress and high suture stresses (Perktold et al., 2002) leading to anastomotic Intimal hyperplasia (AIH) (thickening on the inner wall of a blood vessel) (Schiller et al., 2010). Zilla, Bezuidenhout and Human (2007) also highlight that the main reason for small to medium sized ($\leq 4 - \leq 7$ mm) graft (SMGs) failure is due to intimal hyperplasia and thrombogenicity. Thus, understanding how the anastomosed region of the artery behaves and deforms under physiological conditions is critical to understanding graft failure.

There is extensive literature on the mechanical characterisation of synthetic grafts including investigations into burst strength, compliance and circumferential stretch as well as suture techniques and applying prestretches to the anastomosed artery. A range of optical methods have been successfully explored to characterise these properties; however, most investigations seem to omit viewing the internal geometry of the vessel under a variety of pressures. As the internal geometry affects the aforementioned flow conditions, this is deemed to be an important property of the reconstructed vessel.

This study therefore aimed to gain a better understanding of how an anastomosed specimen (Figure 1) deforms under a variety of internal pressures and pretensions. Additionally, it was investigated how the anastomosis and specifically the tension in the sutures distorted the specimen and inhibited normal geometry changes. A synthetic representation of an artery was used in an extension-inflation test that simulated normal physiological conditions. Empirical results were compared to theoretical predictions. 3D representations and cross-sectional images of the specimen were also obtained from the CT scan and analysed.

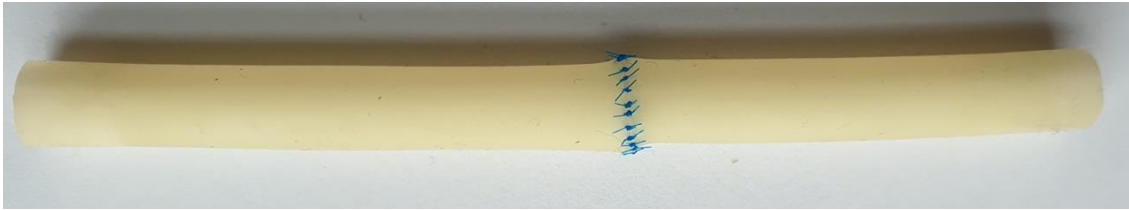


Figure 1: Anastomosed specimen example, Penrose drains sutured

Background

Material Characterisation

In order to predict how the specimen will perform under internal pressure it is necessary to determine the material properties of the synthetic representation first. To do this it is essential to consider the linearity of the material properties. A material can be described as linear elastic “if the force needed to extend or compress it by some distance is proportional to that distance” (Mihai and Goriely, 2017). For linear elastic materials, the most important constants can be summarised as the Elastic Modulus (E) and the Poisson’s ratio (ν). In order for these parameters to remain constant, the material has to obey infinitesimal strain theory and thus only have small deformations relative to its body. If a body experiences large deformation, it then obeys finite strain theory (large deformation theory) and the aforementioned properties will no longer remain constant.

Non-linear elastic bodies such as elastomers (materials with rubber-like properties) display large, non-linear elastic deformation and therefore it is no longer appropriate to model them using constants for Elastic modulus and Poisson’s ratio as they vary as a function of the deformation (Mihai and Goriely, 2017). Hyperelasticity (i.e. non-linearly elastic) is used to model materials such as these (Sasso, Palmieri, Chiappini and Amodio, 2008) where the stress-strain relationship for materials such as elastomers and soft tissue is unique (Mihai, Chin, Janmey and Goriely, 2015). Therefore, in this investigation varying the Elastic Modulus and Poisson’s Ratio as a function of the deformation was attempted because the specimens appear to obey finite strain theory.

Poisson’s ratio is defined as the ratio of lateral deformation to the elongation of a body. It ranges between 0.2 and 0.5 for linear elastic materials and is often measured when the body is experiencing small deformations (Sanborn and Song, 2019). Theoretically, with a Poisson’s ratio $\nu = 0.5$, the material can be described as ‘incompressible’, however experimentally all materials are compressible, and Poisson’s ratio will only ever approach 0.5 (Mott, Dorgan and Roland, 2008).

The Elastic Modulus is defined as stress/strain. It is the measure of elasticity of a body and therefore the ability to resist deformation under load (Roeder et al., 1999).

Once calculated, the Elastic modulus and Poisson’s ratio could then be used to make accurate predictions for changes in geometry of the specimen. The following equations assume a cylindrical specimen.

$$\text{Stress } \sigma \text{ (MPa)} = \frac{\text{Force } F}{\text{Area } A}$$

[1]

$$\text{Longitudinal strain } \varepsilon_{long} = \frac{\Delta l}{l_o} \quad [2]$$

$$\text{Elastic Modulus } E \text{ (GPa)} = \frac{\sigma}{\varepsilon_{long}} \quad [3]$$

From these parameters, Poisson's ratio can be calculated.

$$\varepsilon_{long} = \frac{\Delta l}{l_o} \quad [4]$$

$$\varepsilon_{lat} = \frac{-\Delta\phi}{\phi_o} \quad [5] \text{ [1-5(Philpot, 2014)]}$$

$$\text{Poisson's ratio } \nu = -\frac{\varepsilon_{lat}}{\varepsilon_{long}} \quad [6] \text{ (Sanborn and Song, 2019)}$$

Longitudinal stretch and strain are considered to be positive and therefore the thinning of the lateral dimensions along with the lateral strain is considered to be negative.

Basic Mechanical Predictions

Below is a summary of equations that are used to calculate the predictions in deformations for thin-walled and thick-walled cylinders.

Arteries (both real and synthetic) form a cylindrical shape. Thus, mechanical formulas describing cylinders can be used as a simplified model to predict the stress that their walls are exposed to and to predict their geometric behaviour under pressure.

Thin-walled cylinder subject to internal pressure

$$P = \text{pressure} \times \text{area} = p \times \pi d^2 / 4 \quad [7]$$

$$\text{Area} = \pi d \times t \quad [8]$$

$$\text{Longitudinal Stress } \sigma_L = \frac{\text{Force}}{\text{Area}} = \frac{\left(p \times \frac{\pi d^2}{4} \right)}{\pi d t} = \frac{pd}{4t} \quad [9]$$

$$\text{Circumferential stress } \sigma_H = \frac{pd}{2t} \quad [10]$$

(Hulse and Cain, 2001)

$$\text{Longitudinal strain} = \frac{1}{E} (\sigma_L - \nu\sigma_H) \quad [11]$$

$$\text{Change in length} = \frac{1}{E} (\sigma_L - \nu\sigma_H)L = \frac{pd}{4tE} (1 - 2\nu)L \quad [12]$$

$$\text{Change in diameter} = d\varepsilon_H = \frac{d}{E} (\sigma_H - \nu\sigma_L) = \frac{pd^2}{4tE} (2 - \nu) \quad [13]$$

Thick-walled cylinder subject to internal pressure

$$\text{Radial stress, } \sigma_r = -p \left(\frac{\left(\frac{R_2}{r}\right)^2 - 1}{k^2 - 1} \right) \quad [14]$$

$$\text{Circumferential stress, } \sigma_H = p \left(\frac{\left(\frac{R_2}{r}\right)^2 + 1}{k^2 - 1} \right) \quad [15]$$

$$\text{where } k \text{ is diameter ratio } \frac{D_2}{D_1} = \frac{R_2}{R_1} \quad [16]$$

$$\text{Longitudinal stress } \sigma_L = \frac{p_1 R_1^2 - p_2 R_2^2}{R_2^2 - R_1^2} \quad [17]$$

$$\text{Change in diameter, } \Delta D = \frac{2r}{E} (\sigma_H - \nu\sigma_r - \nu\sigma_L) \quad [18]$$

$$\text{Change in length, } \Delta L = \frac{L}{E} (\sigma_L - \nu\sigma_r - \nu\sigma_H) \quad [19]$$

(Hearn, 1997)

Existing literature

Distensibility is a term used to quantify the properties of arteries. It is defined as the relative change in artery volume for a known change in internal pressure (Chen et al., 2017). Burton (1954), describes that for a material obeying Hooke's law (where

Elastic Modulus E is constant) the volume distensibility of a cylinder would increase as pressure increases. This idea of “blow out” or “inflation jump” is observed in elastomers. Past the critical “limit-point” instability value, the material will continue to stretch with reduced pressure. With a constant pressure, the stretch will jump to a significantly higher deformation (Goriely, Destrade and Ben Amar, 2006).

This however is not observed in arteries. Chen et al. (2017) report that with an increased blood (internal) pressure the artery walls become thinner and the decreased ratio of thickness to radius leads to a lower arterial volume distensibility. This is supported by Matsuda and He (2002), when a carotid artery exhibited a “typical J-curve”, showing large distensibility at low pressures and reduced distensibility as pressure increases. The J-curve in arteries is common and represents a non-linear stress-strain relationship due to the collagen fibre initially being wavy and then straightening out under load, decreasing the distensibility. Single elastomer materials however do not produce J-curves at physiological pressures (Zhalmuratova and Chung, 2020).

Below is a summary of the existing literature:

- Madhavan et al. (2012) cannulated multi-layer vascular grafts and tested them under pressures of 0-160mmHg in increments of 10mmHg.
- Sonoda et al. (2002) conducted a similar experiment to the one planned for this investigation in which an anastomosis between an ePTFE vascular graft and an artery was created. The test was conducted to determine the intraluminal pressure / internal diameter relationship using a digital x-ray system. Three regions were analysed: the centre of each graft and the anastomosis. The results show that there is a “very low pressure-dependent dispensability over the entire pressure range”.
- Bustos, García–Herrera and Celentano (2016) also highlight the rigidity of grafts when testing a woven Dacron corrugated prosthesis. The grafts were also subject to longitudinal stretches of $\lambda_z = 1.25$ and 1.3 where l is current length and l_0 is original length.

$$\lambda_z = \frac{l}{l_0}$$

[20]

- Sommer et al. (2018) conducted extension-inflation tests on human subclavian and iliac arteries to mimic the physiological loading the arteries are normally under. An elongation of the arteries (axial prestretch) was applied of $\lambda_z = 1.0 - 1.2$, slightly lower than in the work of Bustos, García–Herrera and Celentano (2016).

Methodology

Three sets of experiments were conducted for this paper and are listed below. The tensile tests were conducted initially followed by the Optical Method and the CT Method that were conducted concurrently.

1. Tensile tests to determine the material properties of the specimen used in all subsequent experiments.
2. Tests to demonstrate geometric changes in anastomosed specimens as a function of applied internal pressure and applied axial tension, with geometric measurements taken using a camera and Image-J software (hereafter referred to as the Optical Method).
3. Tests as per (2) above, but with geometric measurements taken using a CT scanner and Osirix Lite software (hereafter referred to as the CT Method).

Determination of synthetic artery material properties

In order to make the accurate predictions for the tubular deformation of each specimen, it was necessary to determine the properties of the synthetic representation used. A tensile test was carried out to obtain accurate values of Elastic Modulus E and Poisson's Ratio ν for later comparisons.

Material Assumptions

- All specimens including specimens used for tensile test, predictions and final tests are assumed to be cut from same extruded part. Therefore, it is assumed:
 - All specimens have the same initial outer and inner diameter.
 - Specimens have the same material properties.
- Wall thickness is uniform.
- Specimen cross-sections are perfectly circular.

Experimental procedure

A tensile test was performed on Natural rubber latex Penrose Drains (BD Medical) without anastomosis to determine the material properties.

Firstly, the measurements for the specimens were taken. Multiple length measurements were taken and averaged. Rings were cut from the specimens and a 12MP camera was used to capture the cross-section of the specimen.

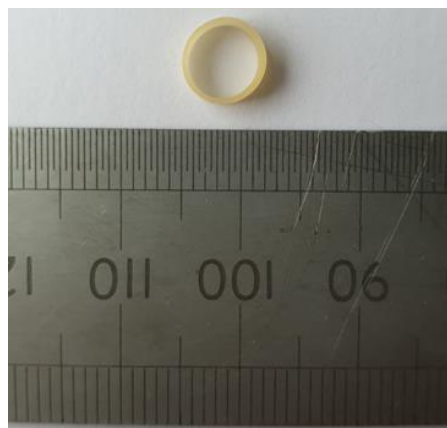


Figure 2: Ring cutting from specimen for Image-J analysis

Image-J (National Institute of Health) image processing software was used to measure and average the outer diameter of the specimen by calibrating the software to a scale in the image (Figure 2). The outer diameter of the specimens was averaged as 7.12mm. The same method was conducted for an average thickness of 0.39mm.

Table 1: Example of initial measurements taken for specimen tensile test

Property	Formula		Value
Inner Diameter (mm)	$ID = OD - (2 * t)$	ID	6.34
Length (Specimen 1) (mm)		$= 7.12 - (2 * 0.39)$	87

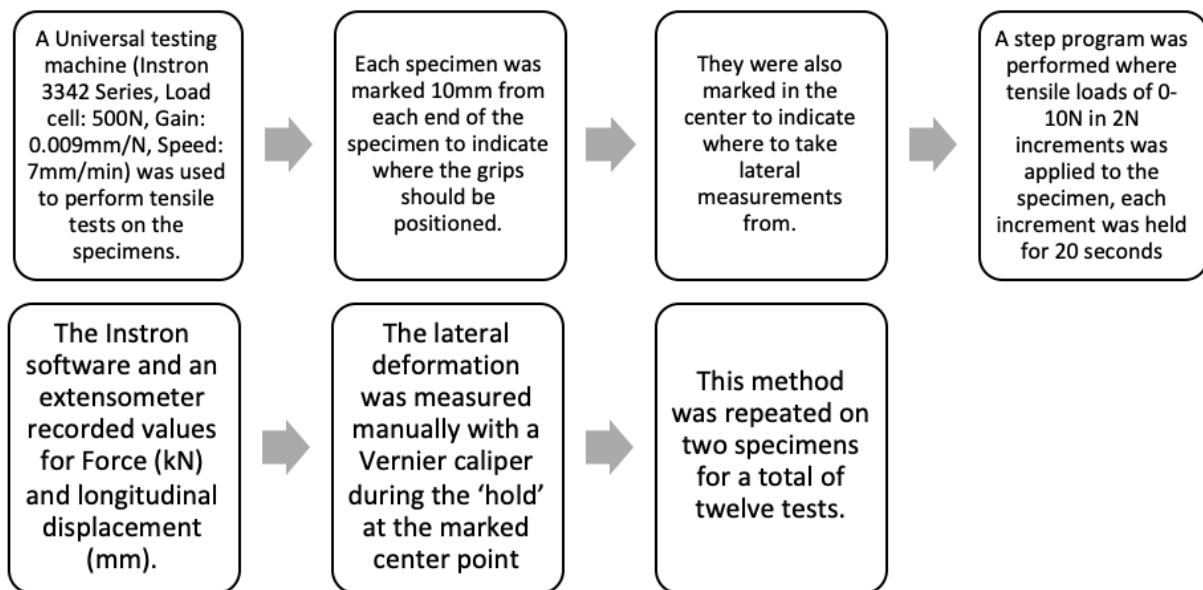


Figure 3: Flow chart of Tensile test procedure, which outlines how the tensile test was conducted.

Using equations [1-5] properties of the specimen were calculated.

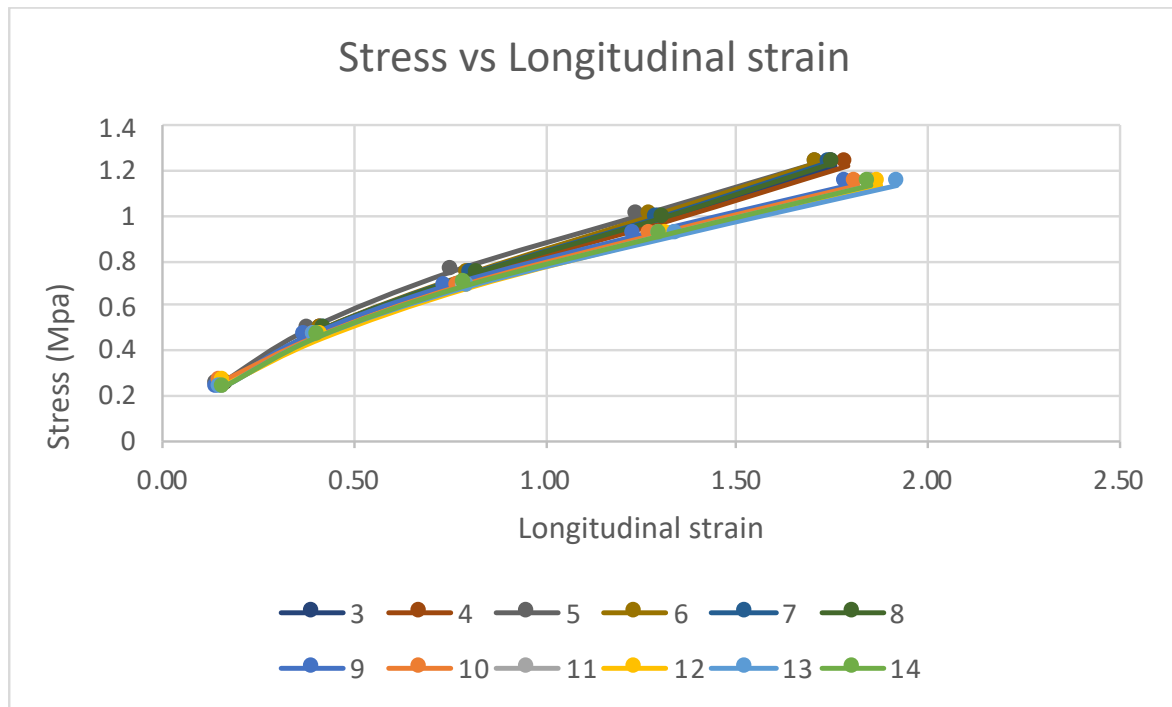


Figure 4: Tensile test, Stress-Strain Curve for tests 3-14

A stress-strain curve was plotted for all twelve specimens (Figure 4). It was evident from the stress-strain curve, that the specimen was not displaying linear characteristics. An average of all tensile tests was taken to determine a function for elastic modulus so that its variation with stress can be calculated (Figure 5).

In the next section, using the tensile test data, an attempt was made to evaluate the variation in Elastic modulus and Poisson's ratio as a function of stress in order to apply this to the theoretical predictions of tube deformation under pressure.

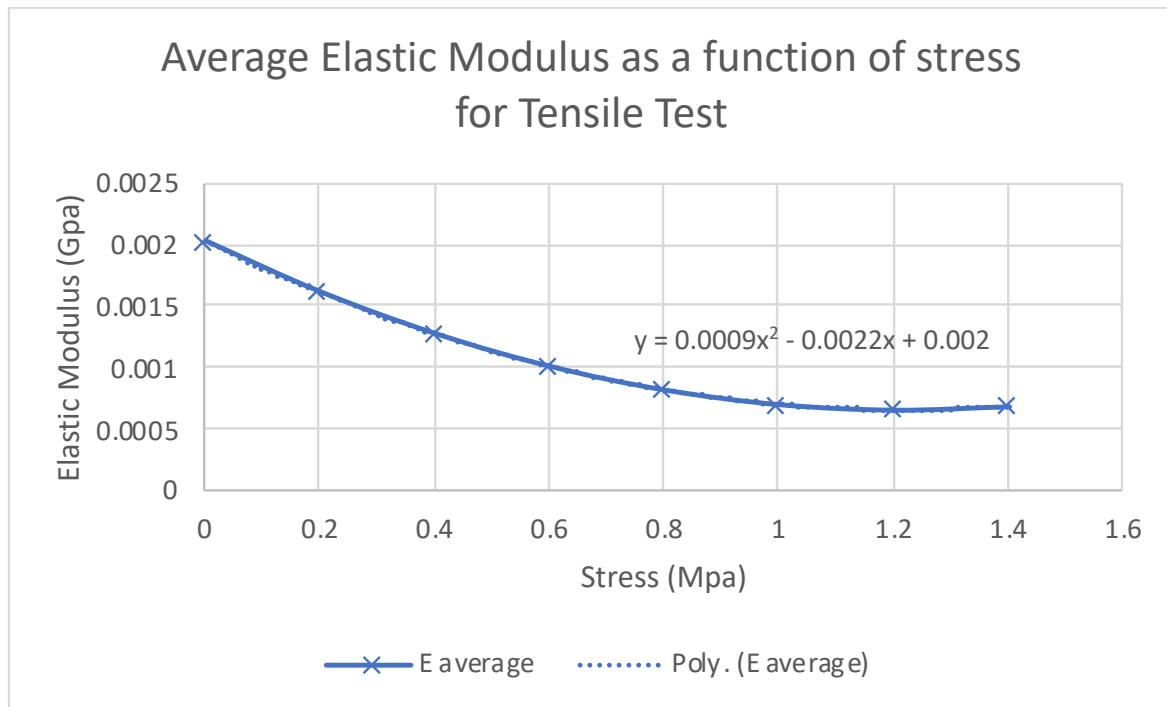


Figure 5: Tensile Test, Average of all tests for Elastic Modulus as a function of Stress

The equation of the curve for the tensile test was applied to the theoretical predictions to predict how the Elastic Modulus would vary with stress.

The coefficients of the 2nd order polynomial equation for Figure 5 are defined as:

$$y = 0.000907716x^2 - 0.002218145x + 0.00201628 \quad [21]$$

Equation 21 dictates how the Elastic Modulus varies with stress in the tensile test. The equation was applied to the prediction calculations so that Elastic Modulus varied (Figure 6).

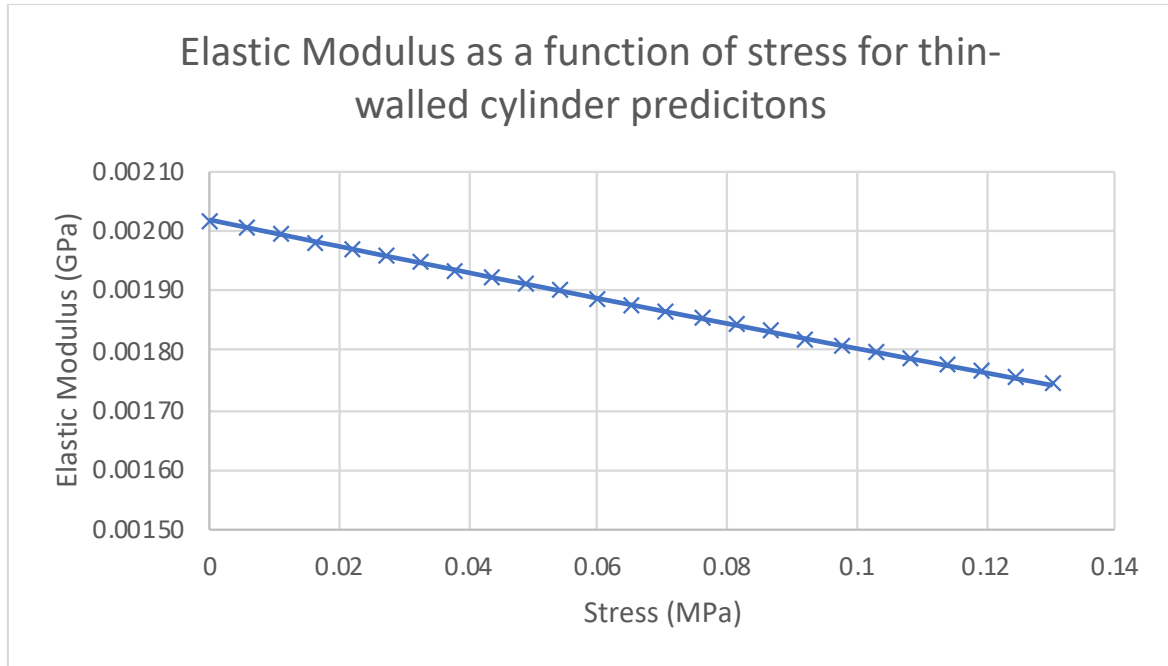


Figure 6: Predictions, Thin walled cylinder. Elastic Modulus as a function of stress, showing how elastic modulus varies with stress in the predictions.

Note that the stresses in predictions (Figure 6) are for a range of pressures 0-240mmHg and consequently the stresses are far lower than that of the tensile test (Figure 5). The non-constancy of the Elastic modulus provided more accurate predictions of how the specimens would deform circumferentially and longitudinally.

The same method was carried out for Poisson’s ratio. An average of all tensile tests was calculated and plotted on Figure 7 as a function of stress.

The equation of the curve for the tensile test was applied to the theoretical predictions to predict how Poisson’s Ratio would vary with stress.

The coefficients of the 2nd order polynomial equation for Figure 7 are defined as:

$$y = 0.481971383x^2 - 1.197533301x + 0.960674328$$

[22]

Equation 22 dictates how Poisson’s Ratio varies with stress in the tensile test. The equation was applied to the prediction calculations so that Poisson’s Ratio varied.

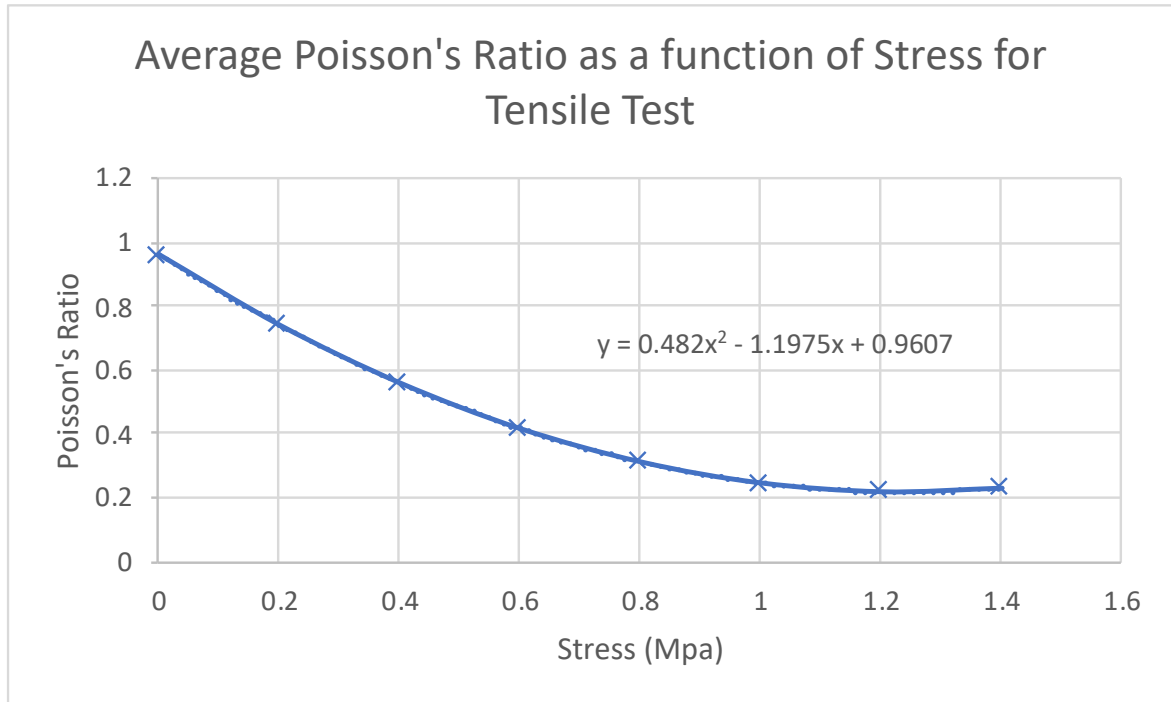


Figure 7: Tensile Test, Average of all tests for Poisson's Ratio as a function of Stress

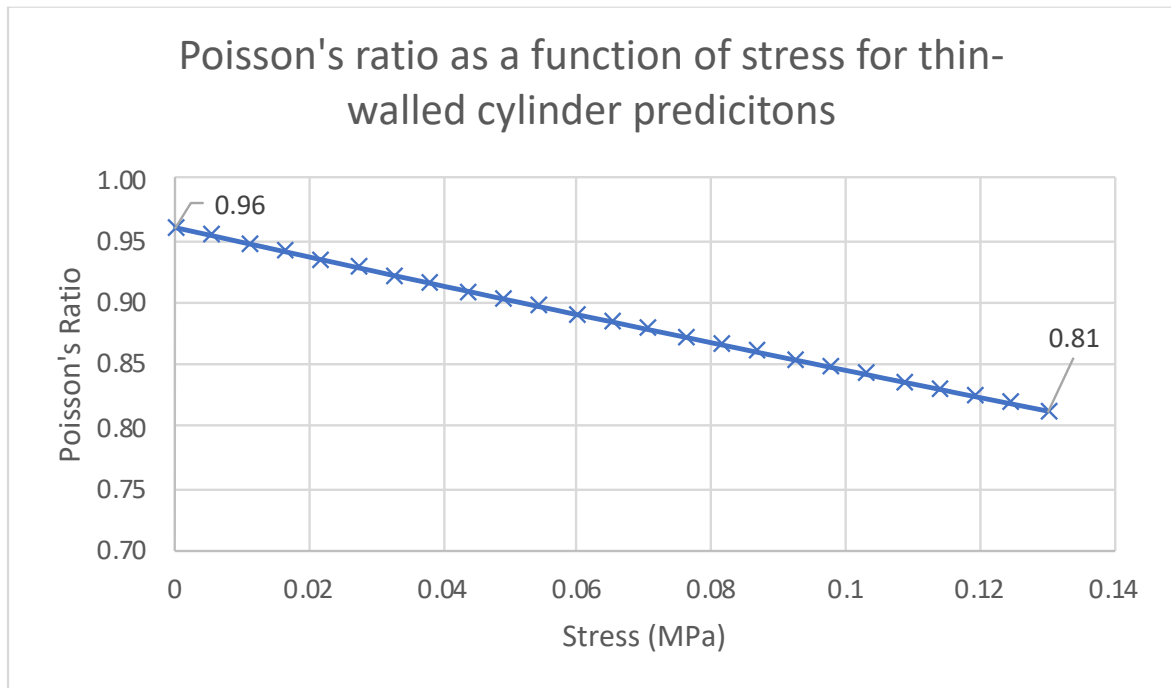


Figure 8: Predictions, Thin walled cylinder. Poisson's Ratio as a function of stress

The equation was used to calculate the Poisson's ratio for the stresses in the predictions. Note that the stresses in predictions are for a range of pressures 0-240mmHg and consequently the stresses are far lower than that of the tensile test.

The same process was also applied to thick-walled cylinder predictions.

Figure 8 shows how Poisson's Ratio varies with stress. Poisson's ratio values of between 0.81 and 0.96 were predicted for the range of physiological pressures. These values are out of the possible range for Poisson's ratio of 0.2-0.5 as discussed earlier. Since the lateral and longitudinal measurements were taken using different methods (manually versus extensometer recordings, respectively), it is likely that different errors were introduced in the two sets of measurements. It's believed that this is the reason for the impossible Poisson's ratio values calculated.

It is most likely that the error in the above data came from the manual measurements of lateral deformation. To get a measure of the error introduced for the lateral measurements, an average diameter of all the tests was taken and diameter plotted as a function of force.

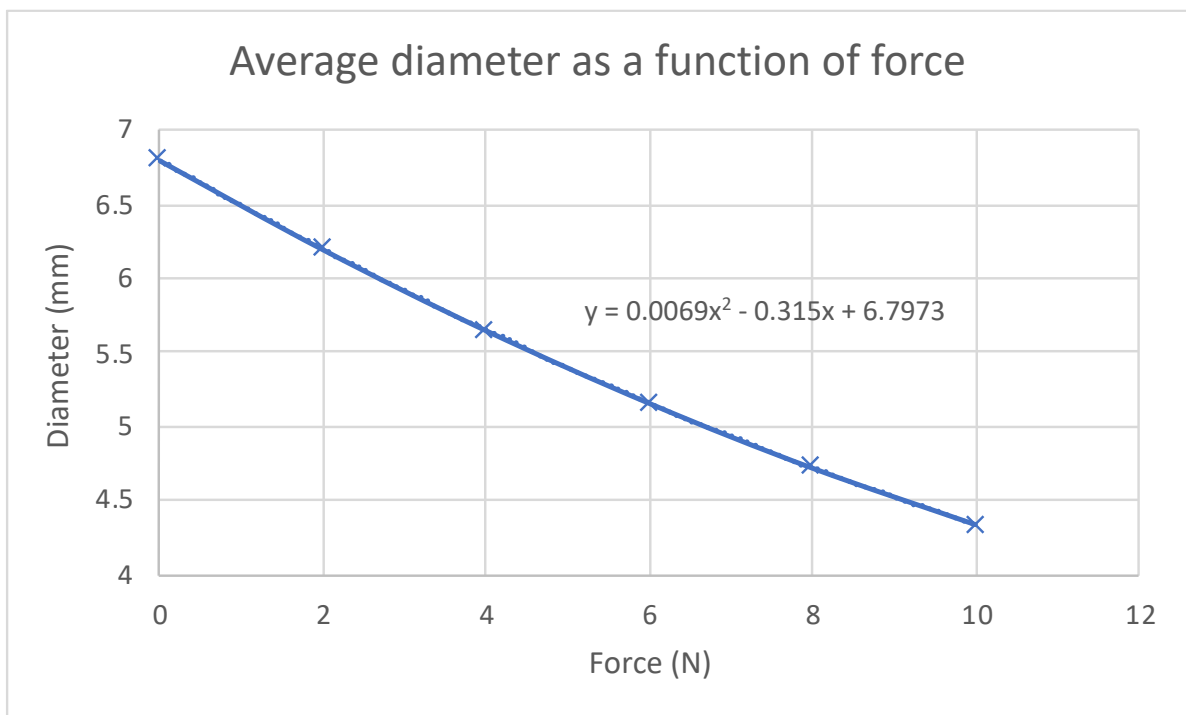


Figure 9: Tensile Test. Extrapolated average diameters as a function of force

The original data for the Tensile test ranged from 2-10N of Force, however the data was extrapolated to a force of zero (Figure 9). This gave an approximation of the original diameter based on the equation of the line. At a force of 0N i.e. original undeformed diameter of the specimen, the extrapolated data predicts a diameter of 6.79mm. Compared to the actual measured original diameter of 7.12mm there is a percentage difference of (-) 4.63%.

This percentage difference could be a result of measuring the specimen manually and accidentally deforming the specimen to a smaller diameter with the Vernier callipers. Alternatively, it could reflect inaccuracy in the initial measurements. It may also arise from the data not being appropriate to extrapolate.

Figure 8 & Figure 9 show the sensitivity of the experiment when taking measurements manually. Since an inaccurate Poisson's Ratio was predicted, a

constant value for Poisson's ratio was used. As discussed in Introduction and Background, although elastomers such as rubber are modelled as 'incompressible', experimentally this is impossible. Therefore, since similar incompressible mechanical properties between the specimen and rubber are expected, a constant Poisson's ratio of $\nu = 0.49$ was used.

Rig Design

Summary of experimental design:

- Conduct a similar rig set up as that described by Madhaven et al (2012) but simplified and less expensive.
- Pressure range for this investigation will ideally be extended from 0mmHg to 240mmHg in order to simulate hypertension and hypertensive crisis (normal blood pressure 120/80mmHg).
- A synthetic representation of an artery will be used with softer mechanical properties than graft material.
- A pretension will also be applied to the anastomosed vessel to simulate the conditions arteries are under in the body.
- CT scanning the experimental procedure will allow both an image of the change in diameter as well as producing 3D DICOM format images, allowing construction of cross-sectional slices.

The principle of the rig is to provide pressurised water to the specimen by applying and varying weight to a syringe. A pretension will be imposed on the specimen to simulate the tension arteries would be under in the body. Pretensions of $\lambda_z = 1.05, 1.16$ and 1.25 were investigated where,

$$\lambda_z = \frac{l}{l_0} \quad [23]$$

(Bustos, García-Herrera and Celentano, 2016)

Figure 10 & Table 2 outline the working principles of the rig.

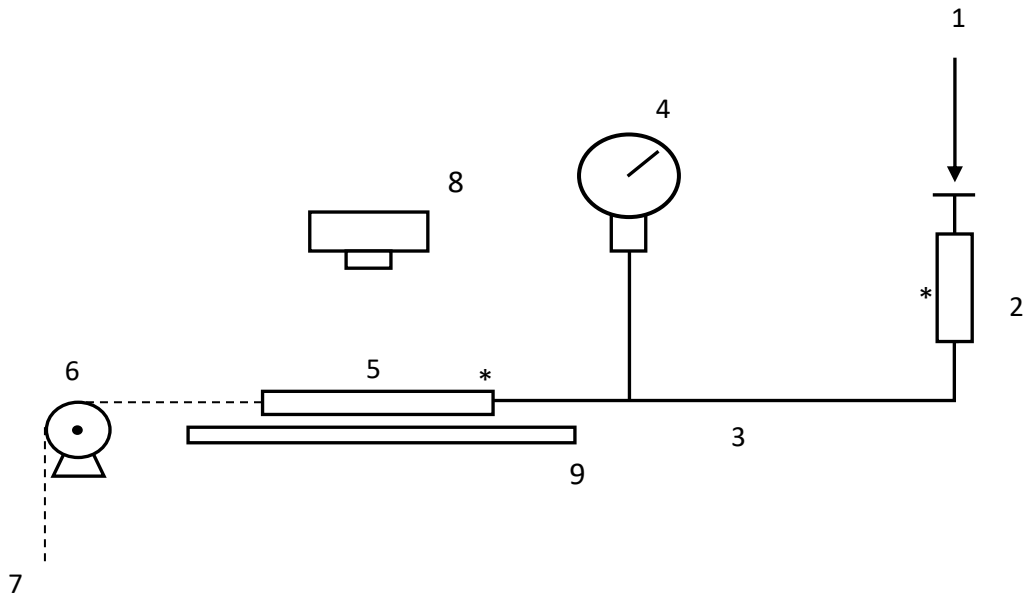


Figure 10: Schematic of rig set up

Table 2: Schematic Key for items and purpose

Number	Item	Purpose
1	Weight (varied)	Apply different weights to the syringe to vary the pressure in the system
2	Syringe	Transfer pressurised water to system
3	Connecting tubes	Transport pressurised water to system
4	Digital Manometer	Measure pressure in the system
5	Anastomosed Specimen	To be pressurised and measured for deformation
6	Pulley wheel	Translate vertical load to horizontal tension applied to the specimen
7	Weight (varied)	To apply load to the specimen
8	Camera	Image deformation of specimen (Optical method only)
9	Rule	Used for Image processing software calibration (Optical method only)
	-----	Fishing line with attached weight (7)
	-----	Connecting tubes (4)
	*	Clamping points at syringe and at one end of the specimen

For rig set up procedure see Figure 13.



Figure 11: Rig set up for CT method. Prior to 3-way valve addition which was added to refill the syringe



Figure 12: Rig set up for Optical Method – Same as CT set up with addition of clamp to hold camera and steel rule for calibration. 3-way syringe valve also pictured.

Experimental procedure

Whilst setting up the rig, the following was considered:

- Clamp was not tight enough to deform the diameter of the syringe.
- The specimen centre (horizontally) was at the same height (70mm) as the syringe tip.

Experimental Assumptions

- Pressure is constant throughout entire system.
- Only the specimen is deforming due to the pressure.
- No air is present in the system.
- No weight applied as pretension is lost due to stretch in the fishing wire or friction due to the pulley.
- Pretension weight is pulling from the central axis of the bung / specimen.
- Original dimensions for Location 2 (anastomosis) are assumed to be the average of Location 1 and Location 3 i.e. the diameter of the specimens before sutures were added.

Materials used

Table 3: Anastomosed specimen, materials and techniques used

Component	Material / Technique
Material (synthetic representation)	Natural rubber latex Penrose Drains (BD Medical)
Suture material	Approx. 30mm each Non-absorbable Polyamide 6 (Ethilon Suture 8-0, Ethicon / Johnson & Johnson)
Suture technique	Interrupted stitching, followed by a double throw and two single throws.

General Procedures

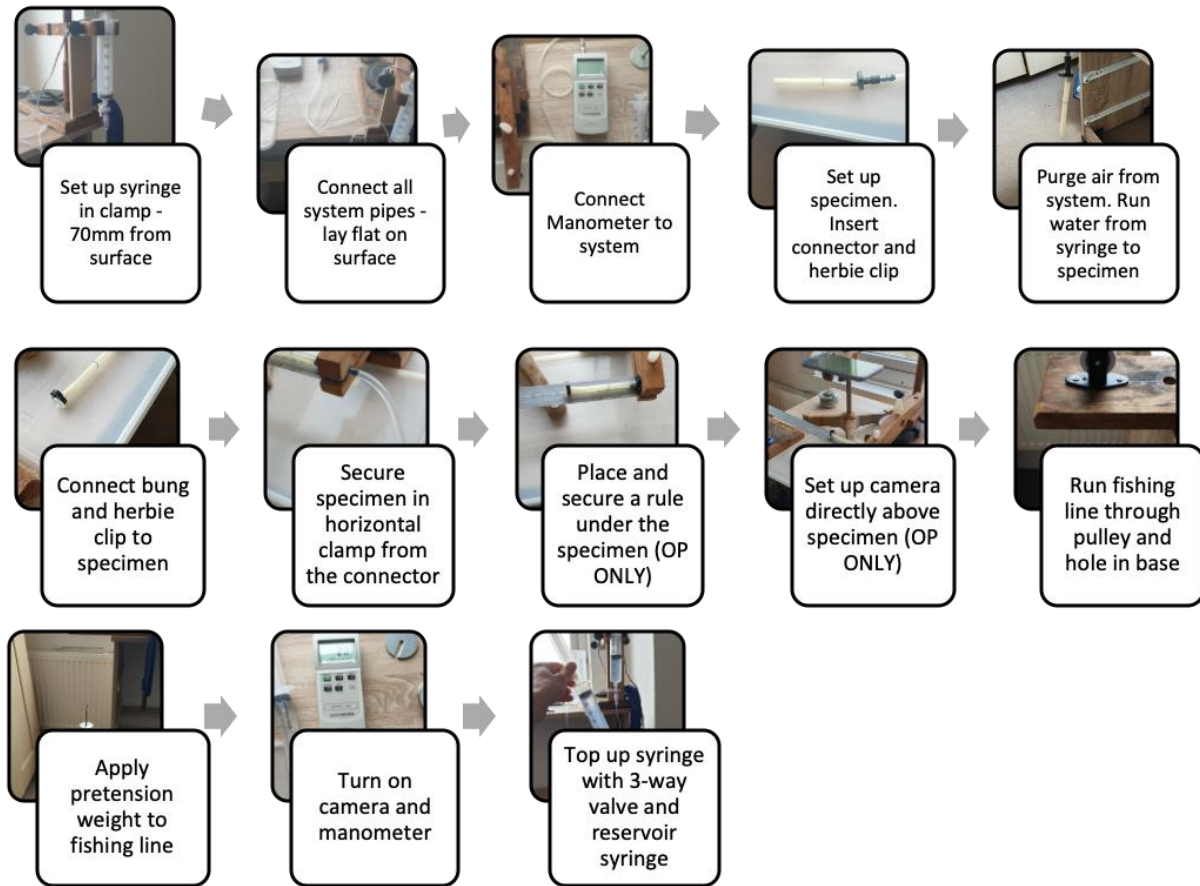


Figure 13: Flowchart of general rig set up procedure

For both methods, CT and Optical, weight was applied in approximately 100g increments. This gave approximate pressure increases of 10mmHg. The pressure was recorded from the Digital Manometer readings. The specimen was imaged with the respective methods and the images were then analysed for changes in diameter and length.

All measurements for diameter, length, area (CT only) and pressure were inputted and analysed in Excel 2020. The percentage changes in diameter, length and area were calculated using the first data point from that experiment as the datum. For example, the first pressure applied (usually around 10mmHg) was used as the datum and changes in geometry we calculated based on the geometric changes from this initial pressure.

For Diameter 2 (Figure 17) the percentage change was calculated using an average of the first data points for Diameter 1 and 3 as a datum. Therefore, the results also show how much the addition of sutures add to the dimensions of the specimen. For the CT method, standard deviation was also calculated for the four diameters taken at each cross-section.

CT Method

A GE Healthcare Discovery CT750 HD Scanner of 0.2mm resolution was used in the investigation. A high radiation dose was used to minimise artefact with an image slice size of 0.625mm. Edge enhancement was used on the images for clarity.

The DICOM files from scans were processed using Osirix Lite DICOM viewer. Predetermined window settings were applied and ‘Bone setting’ provided an image with a diameter and thickness closest to the true value, determined by taking measurements. “Window width (W) determines the range of pixel values that will be incorporated into the display width” (Upstate Medical University, 2020). This method is expected to be the best available technique in analysing the change in geometry of the specimen. It produces a 3D representation of the experiment and cross-sectional slices to allow for measurements. This will allow multiple diameter measurements to be taken and give an average diameter as well as measuring the area of the cross-section. The resolution of the equipment used is also far superior to that of the optical method. The scanner also allows the distortion of the specimen due to the sutures to be imaged clearly.

Figure 14 outlines how to conduct the CT experiment after the rig set up procedure.

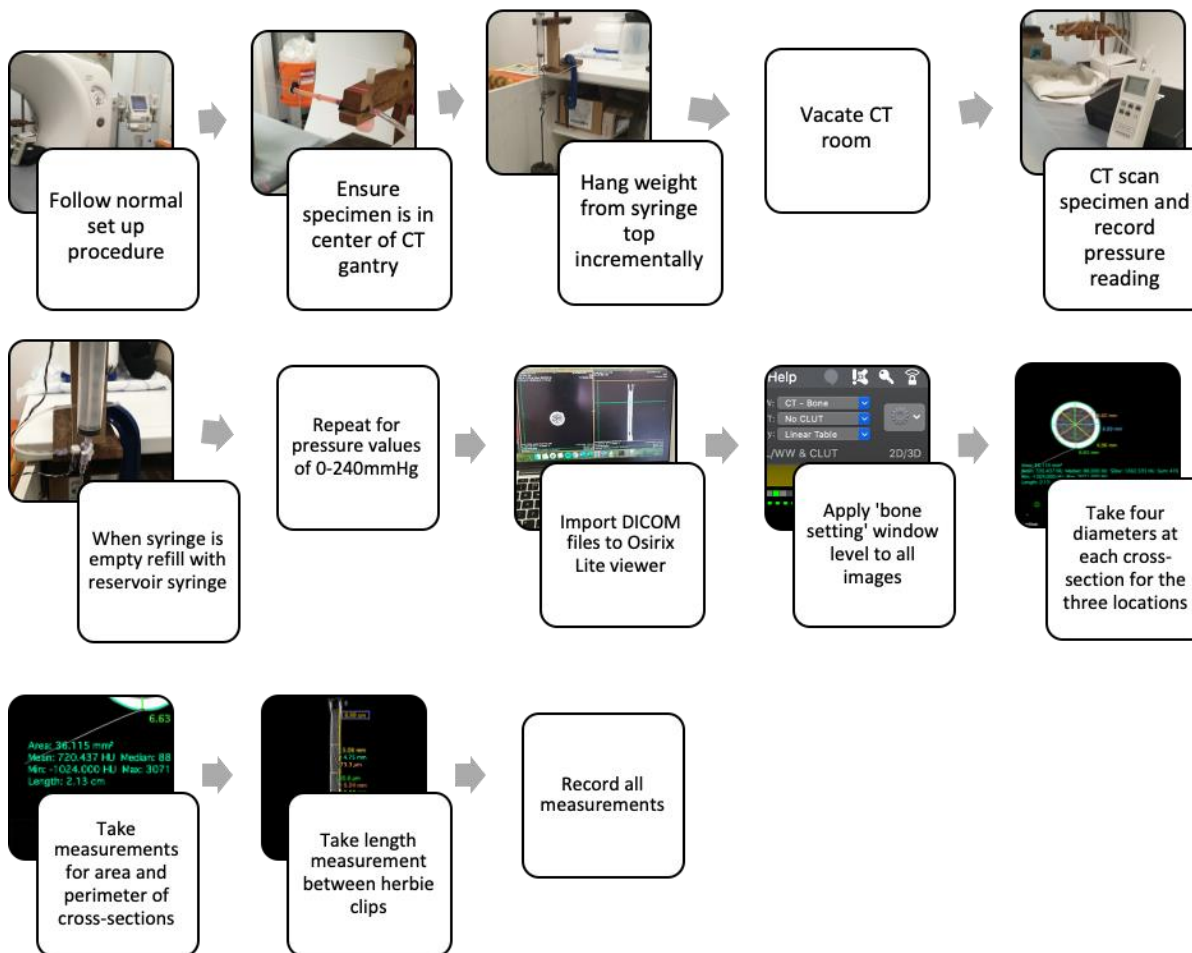


Figure 14: Flowchart of CT method experimental procedure

Figure 15 shows an example of measurements of the cross-sectional slice in Osirix Lite (Left viewer). Right Viewer shows the three locations (Table 4) that diameter and area measurements were taken from. Length measurements were taken between Herbie clips.

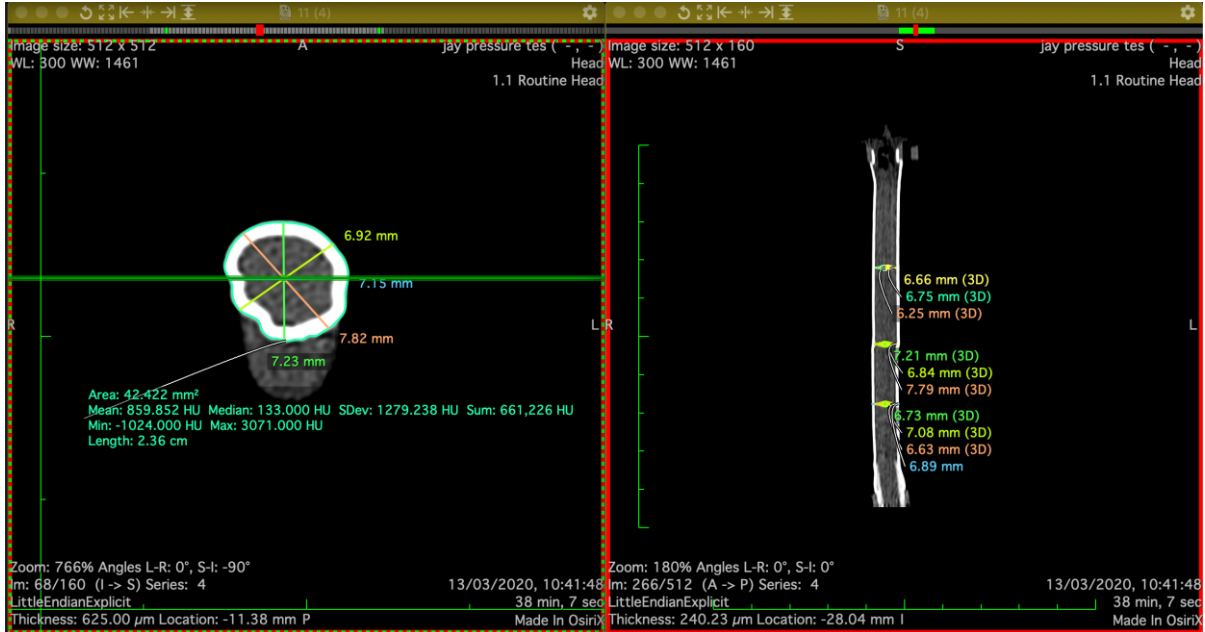


Figure 15: Osirix Lite. Images of vertical and horizontal cross-section of specimen and measurements at 11mmHg. Diameter measurements were taken across 4 axes. Area of cross-section was also measured.

Table 4: Local Osirix Lite Co-ordinates for each cross-sectional slice position

Diameter	Local Co-ordinates (Z)
1	-27
2	-11.38
3	8.63

Optical Method

See Figure 16 for Optical Method procedure.

The Optical method was conducted similarly to the CT method however, at each pressure a 12MP camera was used to image the change in diameter and length of the specimen. The specimen was secured in horizontal orientation with a rule secured directly under.

Image-J software was used to analyse the images. The software was calibrated using the rule and diameter measurements were again taken in approximately the same three locations as the CT method respectively, 50, 70, and 90mm on the rule (Figure 17 and Table 5). Length measurements were also taken between Herbie

clips. Measurements were taken manually, using the software to mark two points and measure the distance between them (Figure 18). This method was also used in order to compare the two methods. The optical method allowed more tests to be conducted as accessibility to the CT scanner was limited.

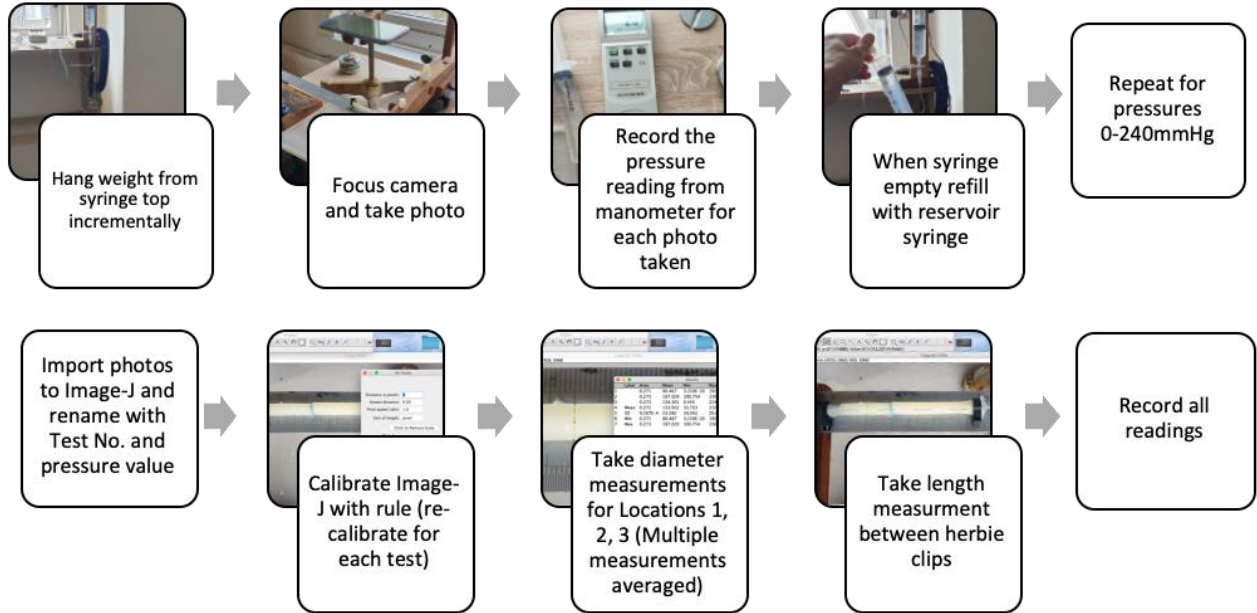


Figure 16: Flowchart of Optical method experimental procedure

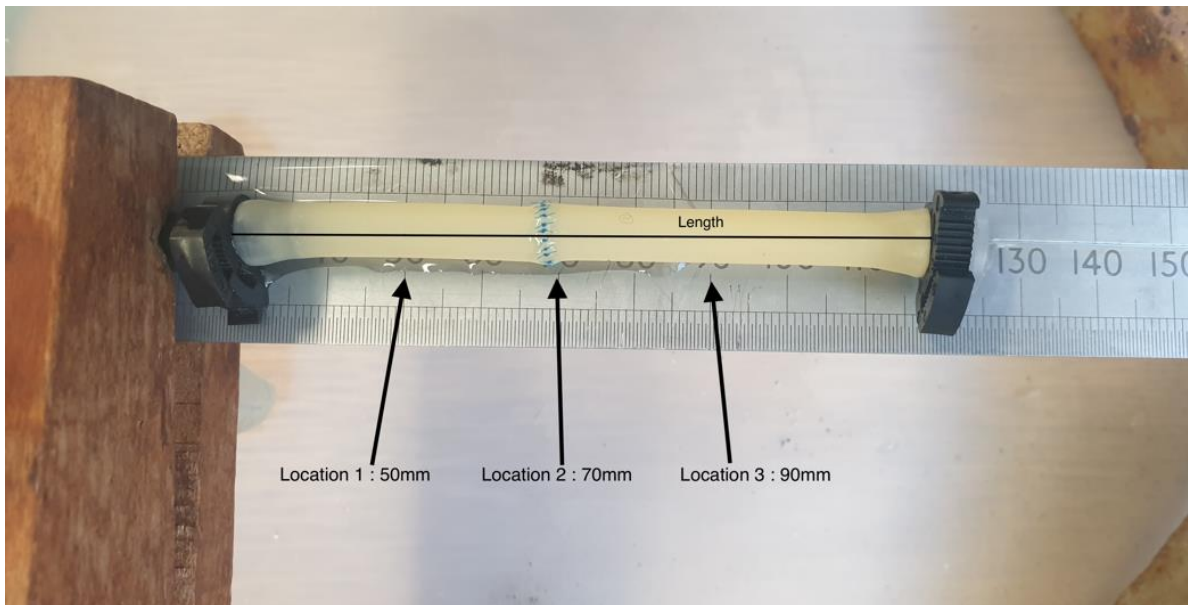


Figure 17: Optical method. Measurement locations for Image-J analysis software.

Table 5: Location and measurement relationship

Location	Measurement (mm)
1	Diameter 1
2 (anastomosis)	Diameter 2
3	Diameter 3
Length	Length

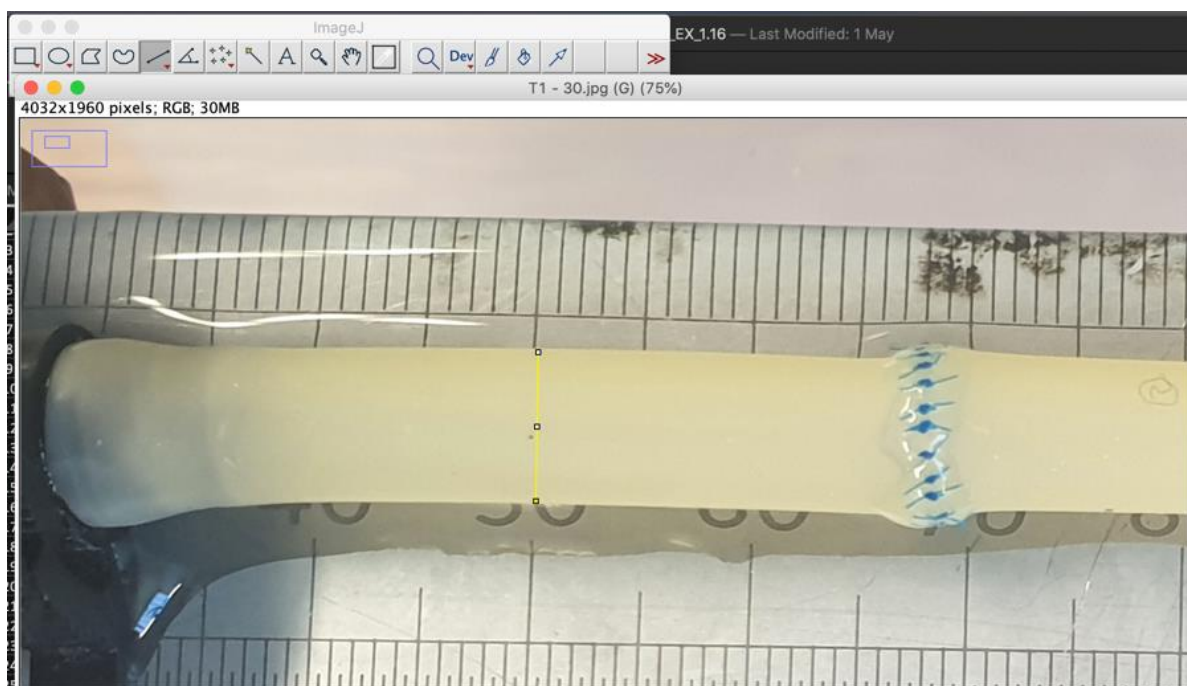


Figure 18: Example of measuring the diameter at Location 1 for Optical method using Image-J software

Note: The location of Diameter 2 is not directly on the sutures. The diameter measurement was taken approximately 2mm from the sutures as they inhibited accurate determination of where the edge of the tube was.

Results

Experimental - CT Method

Table 6: Cross-sectional images of the specimen at the anastomosis region at a range of pressures taken during CT method. Images show the distortion to the specimen caused by the tension in the sutures. As internal pressure increases it is enough to overcome the tension in the sutures, thus making the specimen cross-section more circular.

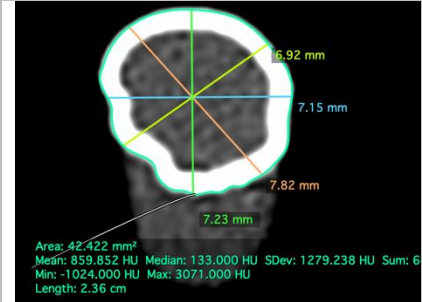
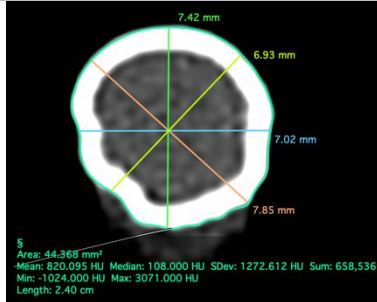
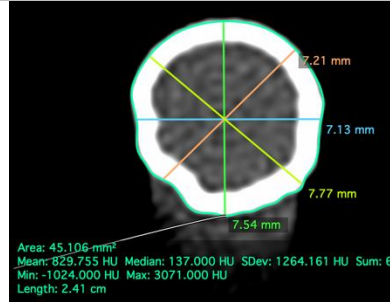
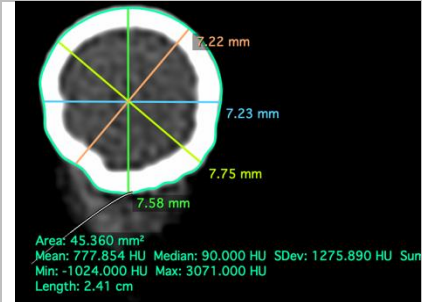
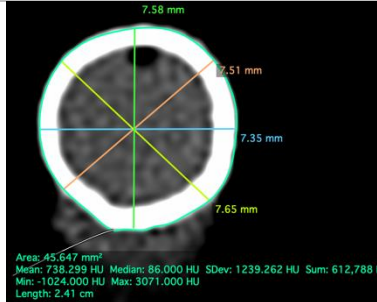
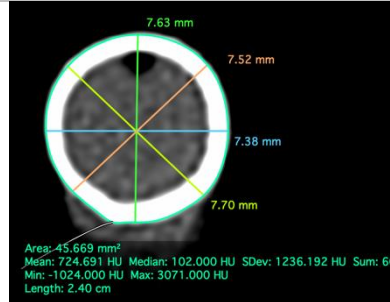
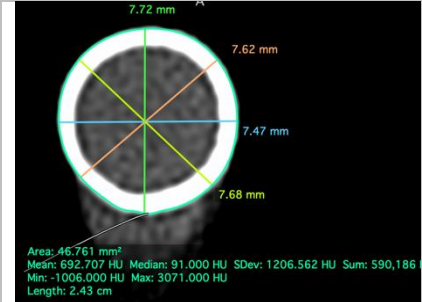
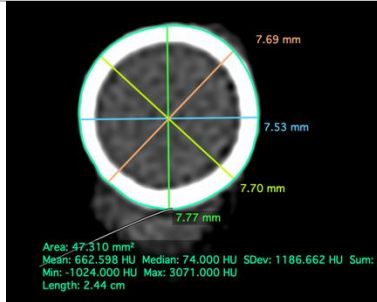
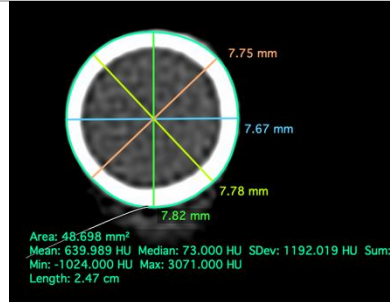
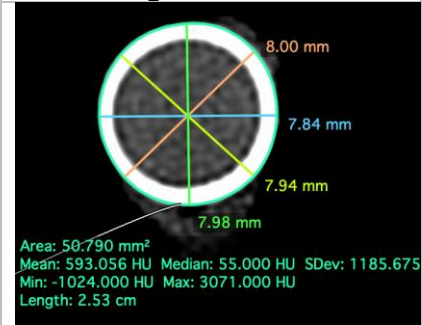
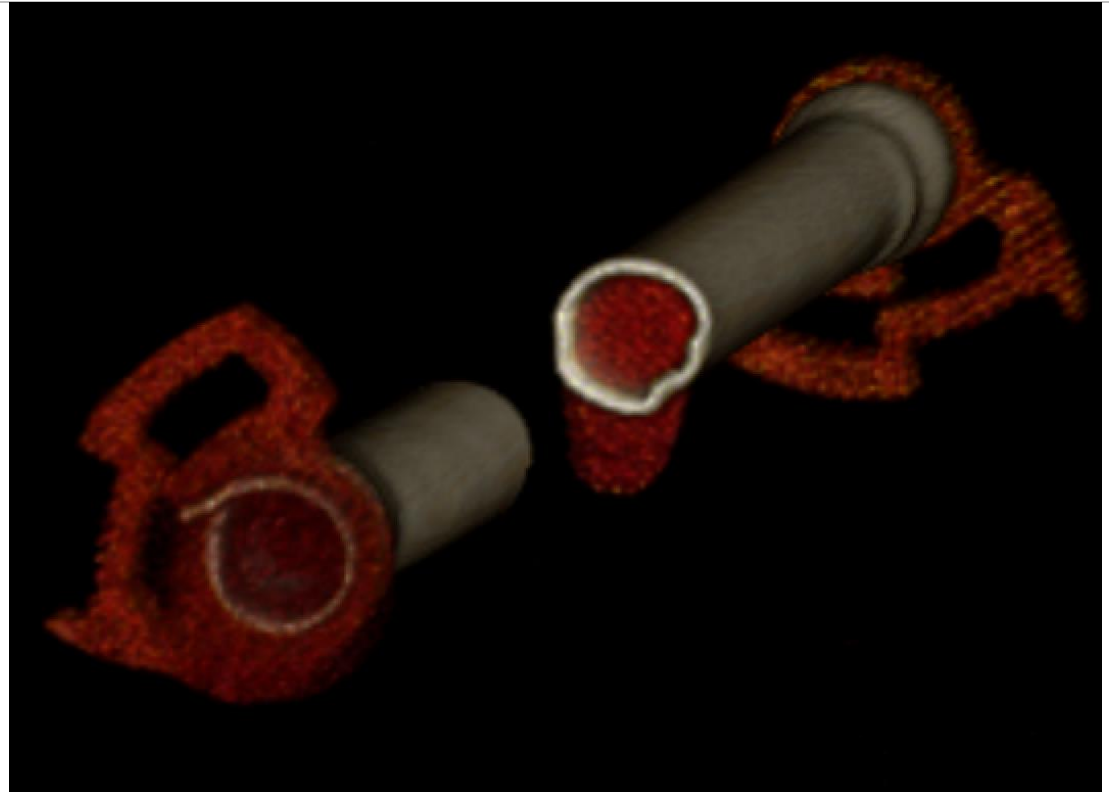
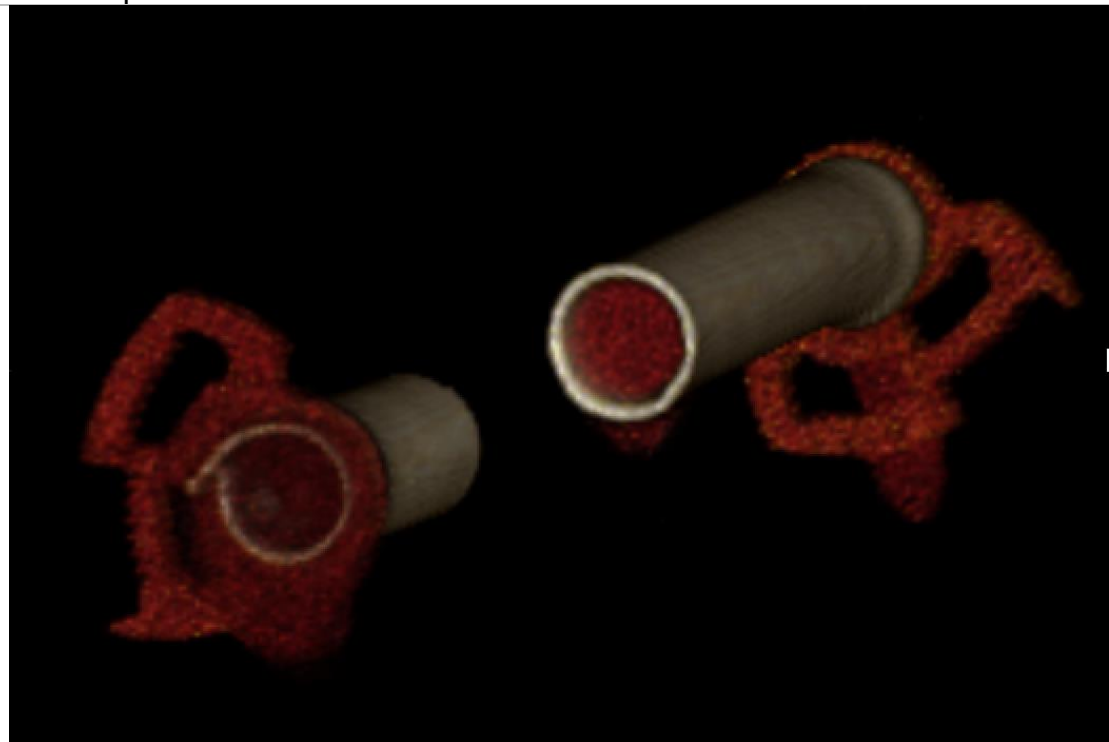
 <p>Area: 42.422 mm² Mean: 859.852 HU Median: 133.000 HU SDev: 1279.238 HU Sum: 6 Min: -1024.000 HU Max: 3071.000 HU Length: 2.36 cm</p>	 <p>Area: 44.368 mm² Mean: 820.095 HU Median: 108.000 HU SDev: 1272.612 HU Sum: 658,536 Min: -1024.000 HU Max: 3071.000 HU Length: 2.40 cm</p>	 <p>Area: 45.106 mm² Mean: 829.755 HU Median: 137.000 HU SDev: 1264.161 HU Sum: 6 Min: -1024.000 HU Max: 3071.000 HU Length: 2.41 cm</p>
11mmHg	29mmHg	53mmHg
 <p>Area: 45.360 mm² Mean: 777.854 HU Median: 90.000 HU SDev: 1275.890 HU Sum: 6 Min: -1024.000 HU Max: 3071.000 HU Length: 2.41 cm</p>	 <p>Area: 45.647 mm² Mean: 738.299 HU Median: 86.000 HU SDev: 1239.262 HU Sum: 612,788 Min: -1024.000 HU Max: 3071.000 HU Length: 2.41 cm</p>	 <p>Area: 45.669 mm² Mean: 724.691 HU Median: 102.000 HU SDev: 1236.192 HU Sum: 6 Min: -1024.000 HU Max: 3071.000 HU Length: 2.40 cm</p>
71mmHg	99mmHg	116mmHg
 <p>Area: 46.761 mm² Mean: 692.707 HU Median: 91.000 HU SDev: 1206.562 HU Sum: 590,186 Min: -1006.000 HU Max: 3071.000 HU Length: 2.43 cm</p>	 <p>Area: 47.310 mm² Mean: 662.598 HU Median: 74.000 HU SDev: 1186.662 HU Sum: 6 Min: -1024.000 HU Max: 3071.000 HU Length: 2.44 cm</p>	 <p>Area: 48.698 mm² Mean: 639.989 HU Median: 73.000 HU SDev: 1192.019 HU Sum: 6 Min: -1024.000 HU Max: 3071.000 HU Length: 2.47 cm</p>
149mmHg	168mmHg	192mmHg
 <p>Area: 50.790 mm² Mean: 593.056 HU Median: 55.000 HU SDev: 1185.675 Min: -1024.000 HU Max: 3071.000 HU Length: 2.53 cm</p>		
240mmHg		

Table 7: Osirix Lite 3D volume renders of the specimen cross-section during CT method. Again, this demonstrates how as the internal pressure increases, the tension in the sutures at the anastomosis is overcome and the cross-section become more circular.



Osirix Lite – 3D volume render cross-sectional slice of specimen at 11mmHg internal pressure



Osirix Lite – 3D volume renders cross-sectional slice of specimen at anastomosis at 192mmHg internal pressure

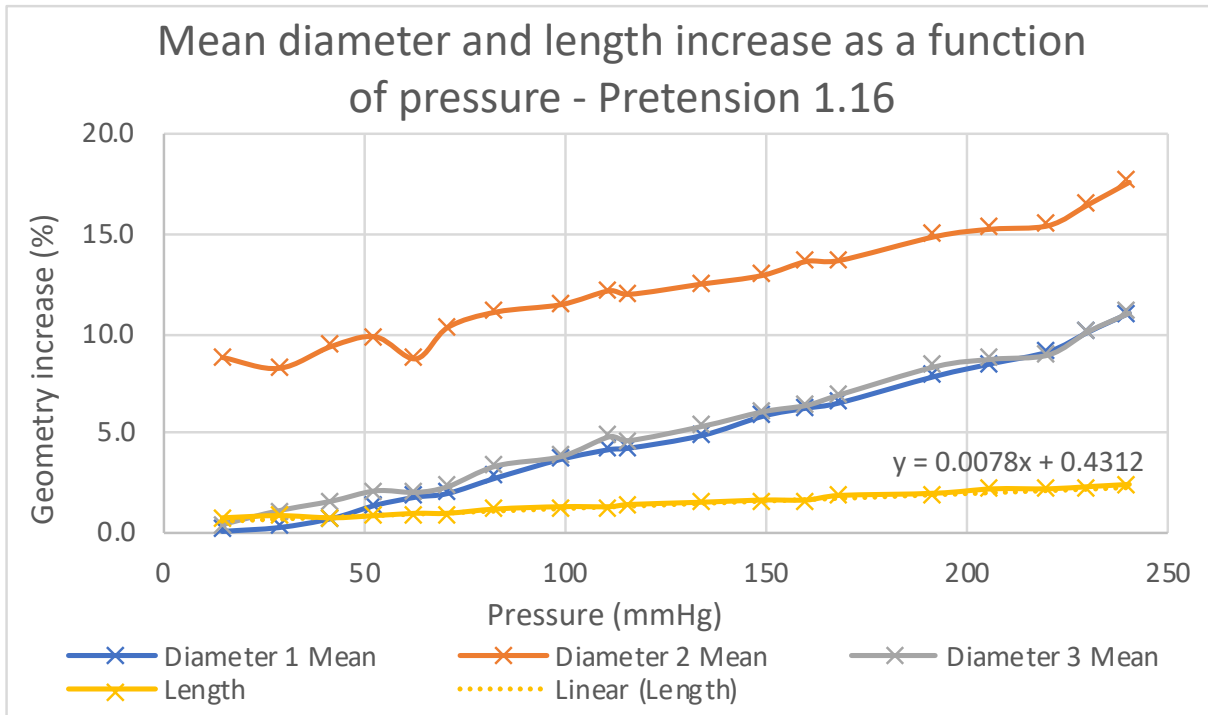


Figure 19: CT Method. Geometry change as a function of pressure. Pretension of 1.16. This shows the increase in diameter and length of anastomosed specimen. The heightened deformation of the anastomosed region is clearly seen.

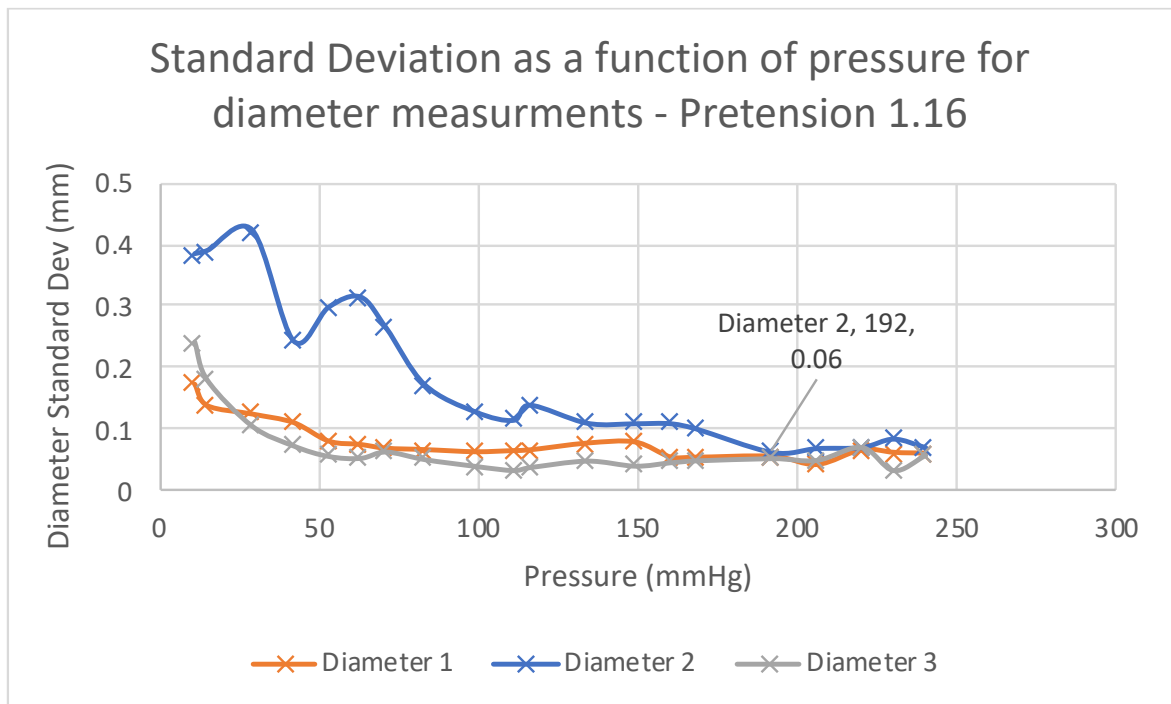


Figure 20: CT Method. SD of diameter measurements as a function of pressure. Pretension of 1.16. Showing more variation (increased SD) for the anastomosed region but an overall decreased variation with increasing pressure for all regions measured.

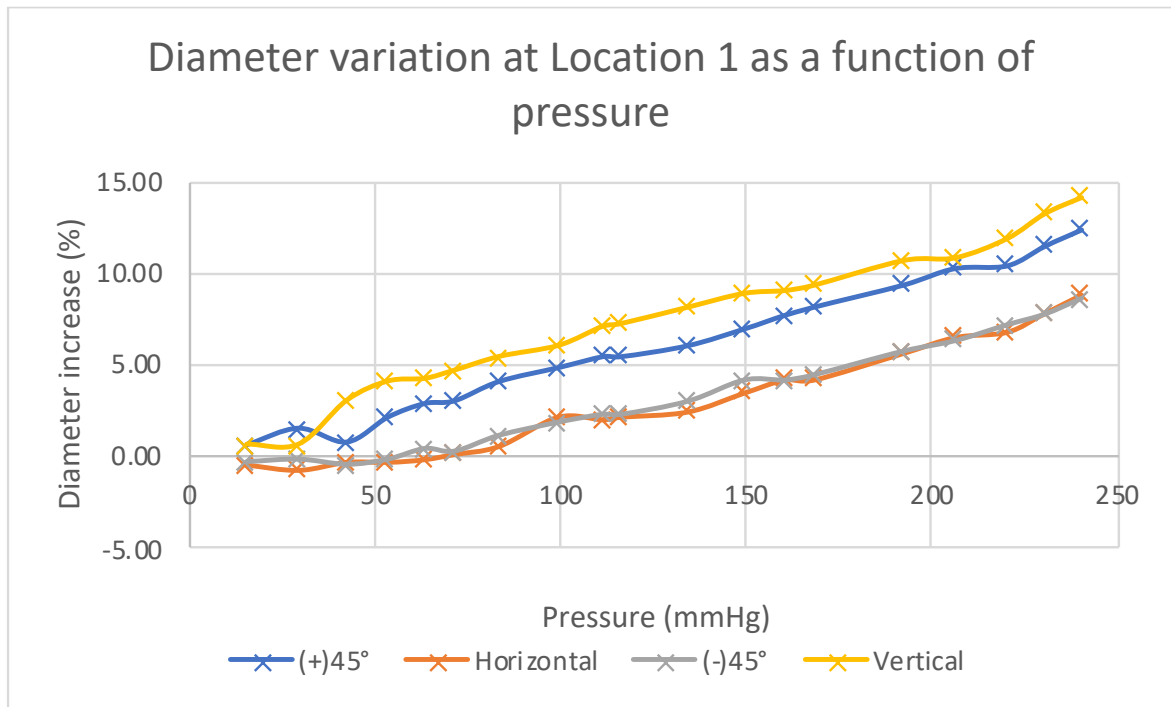


Figure 21: CT Method. Diameter Variation at Location 1 as a function of pressure. Showing diameters measured at different axes. Highlights the importance in taking several measurements to get a better idea of shape/cross section area.

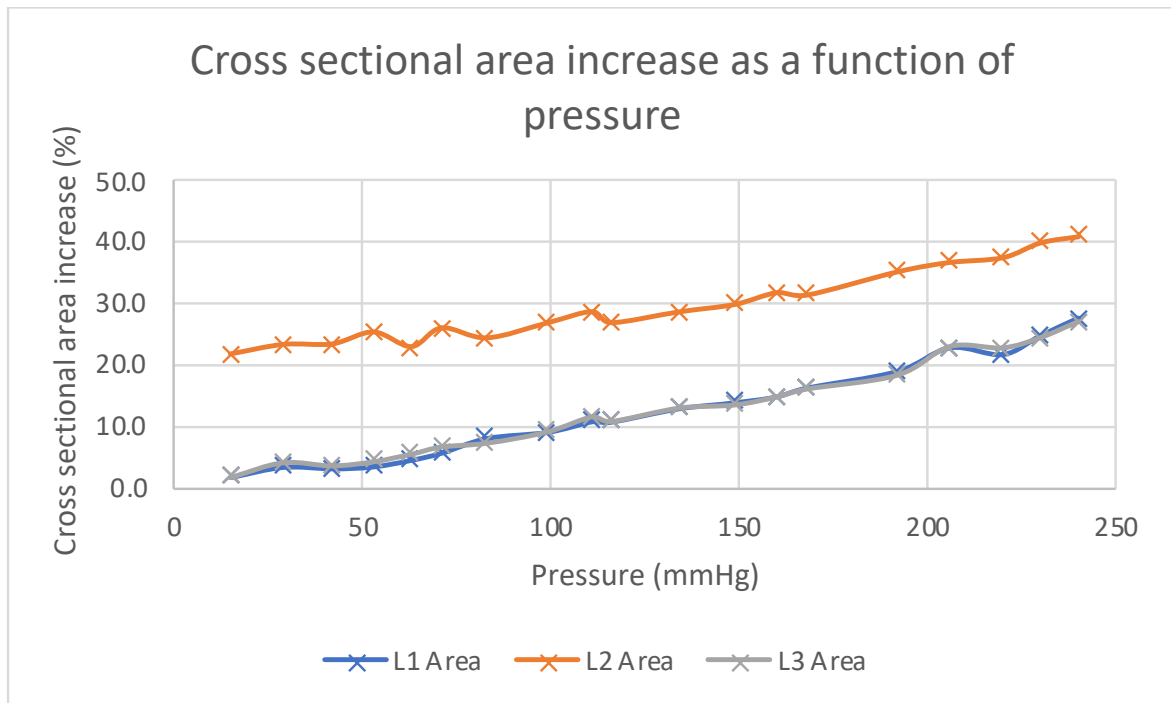


Figure 22: CT Method. Cross section area increases as a function pressure. Showing increase in area at the three locations and almost identical traces for location 1 & 2 highlighting the accuracy of the technique.

Experimental – Optical Method

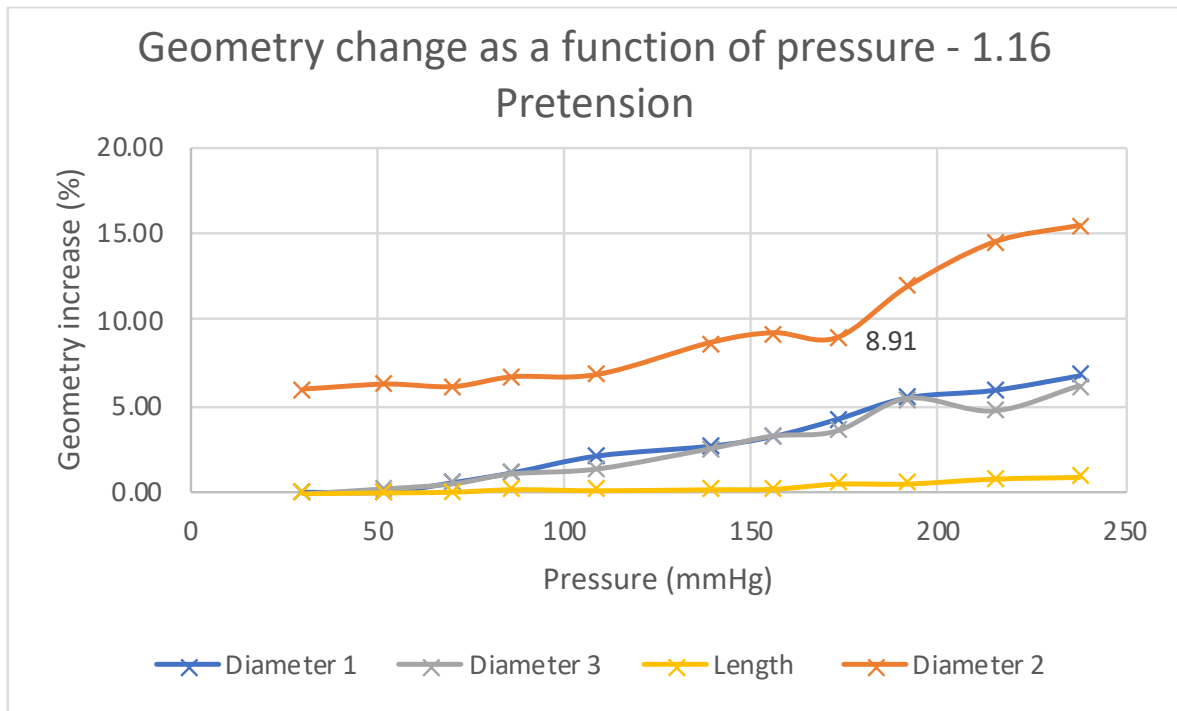


Figure 23: Optical Method. Geometry increase as a function of pressure. Test 1. Pretension 1.16. Confirming CT result, higher geometry changes in the anastomosed region (2).

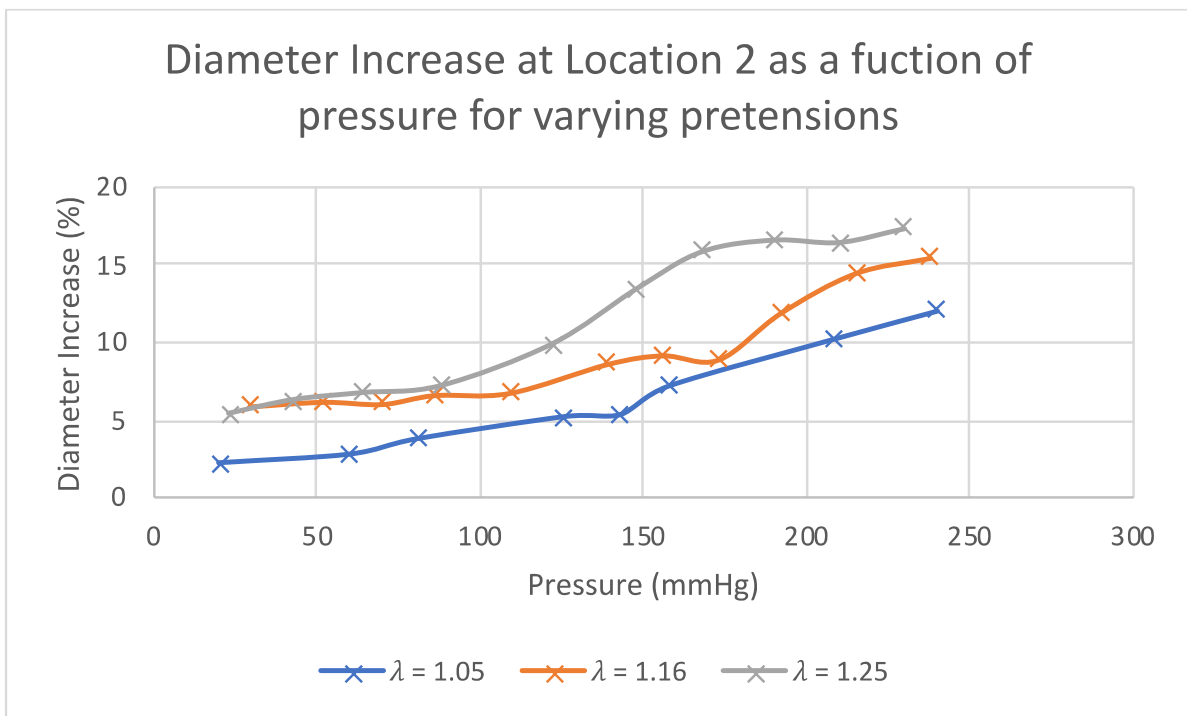


Figure 24: Optical Method. Diameter Increase at Location 2 as a function of pressure for different pretensions. Showing that higher pretensions result in greater diameter deformations.

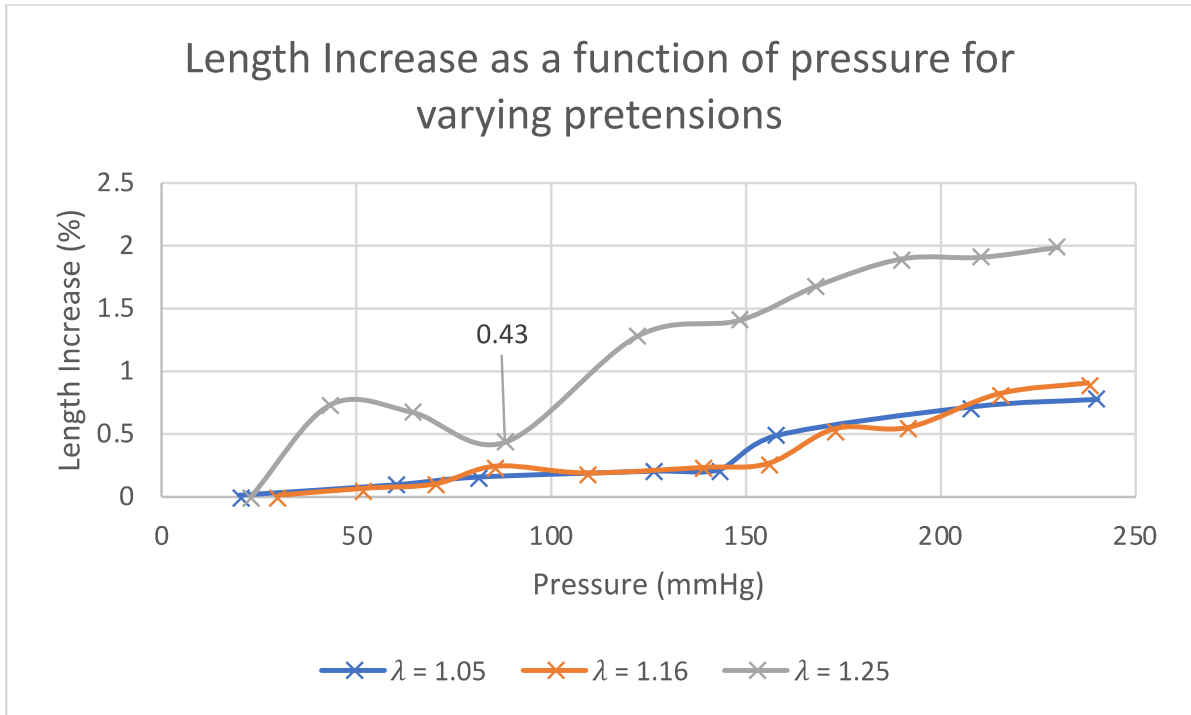


Figure 25: Optical Method. Length Increase as a function of pressure for different pretensions. Shows also that length increases are greater at higher pretensions.

Comparisons

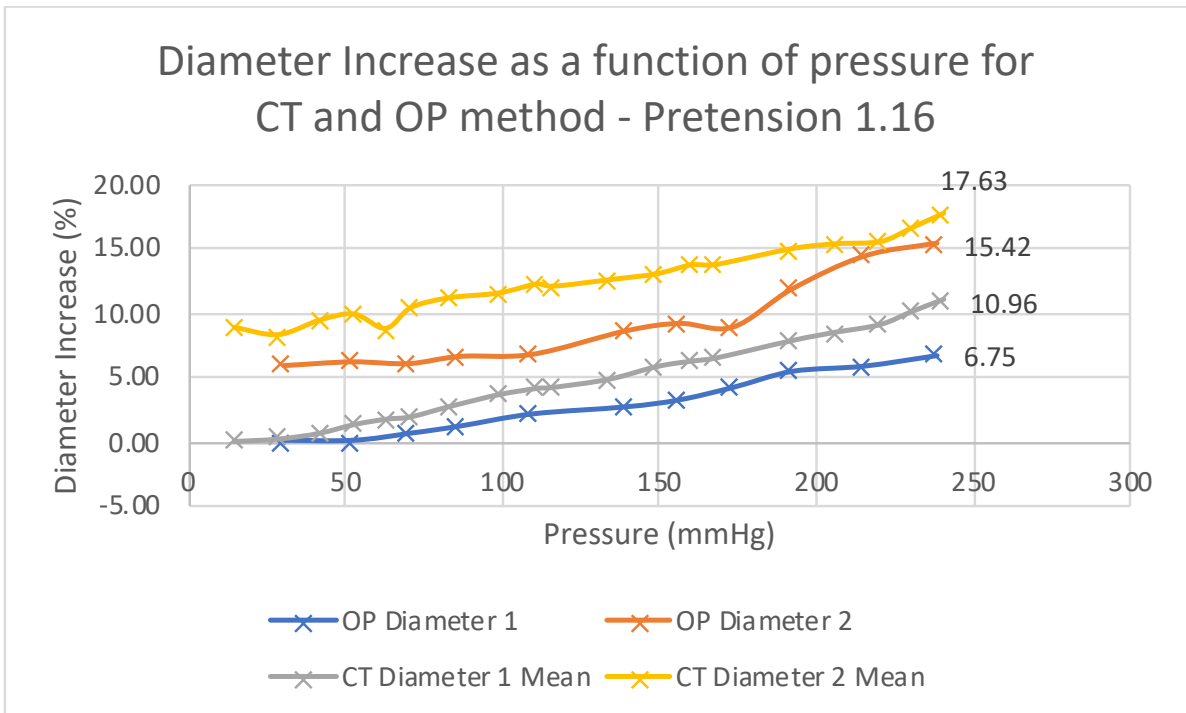


Figure 26: Diameter Increase as a function of pressure for CT and OP method. Pretension 1.16. Shows variation between CT and OP methods. Nonetheless a similar trend was observed, with greater shape changes observed at the anastomosed region compared to region 1.

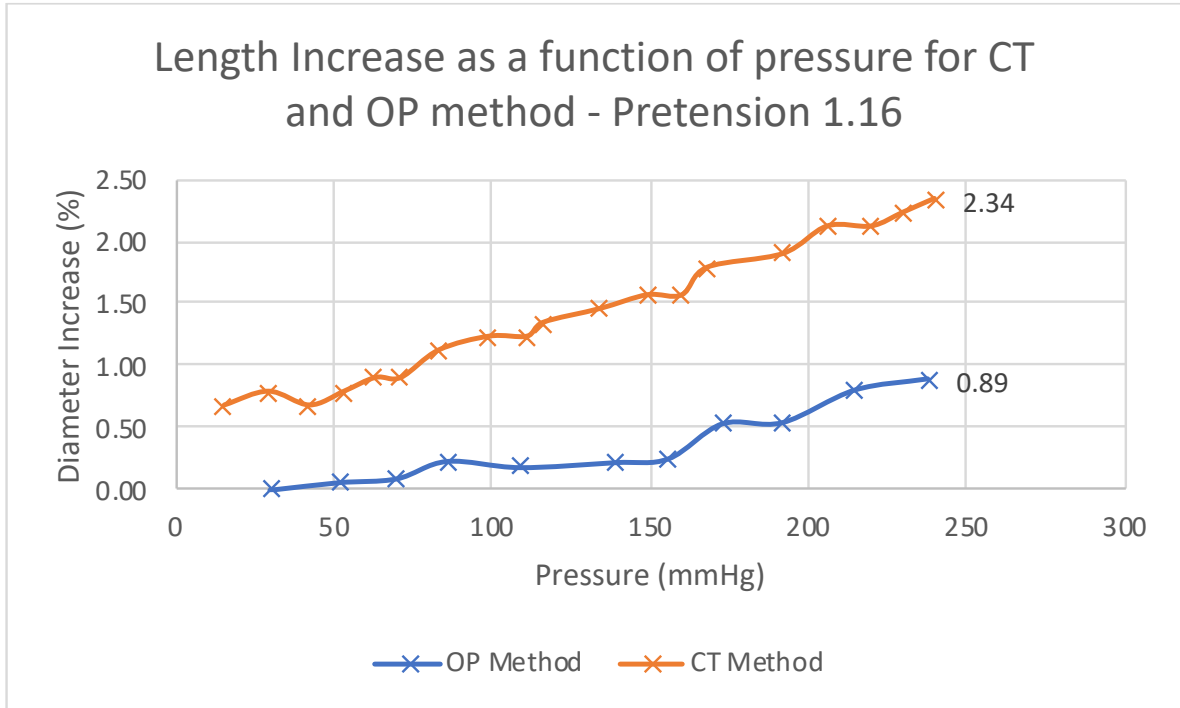


Figure 27: Length Increase as a function of pressure for CT and OP method. Pretension 1.16. Different increases in length measured with different methods.

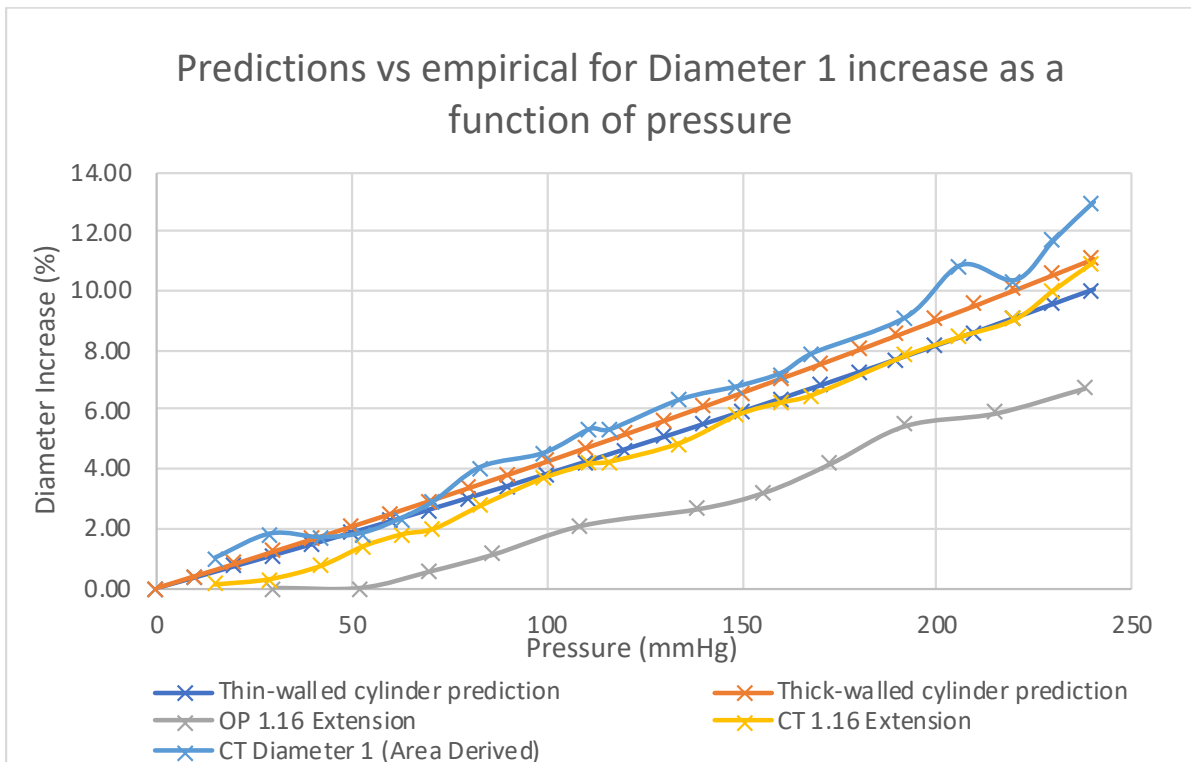


Figure 28: Comparison of predictions and empirical Diameter 1 increase as a function of pressure. Showing that CT measurements fit better with theoretical predictions and therefore believe they are more accurate. CT Diameter 1 (Area Derived) are Diameters derived

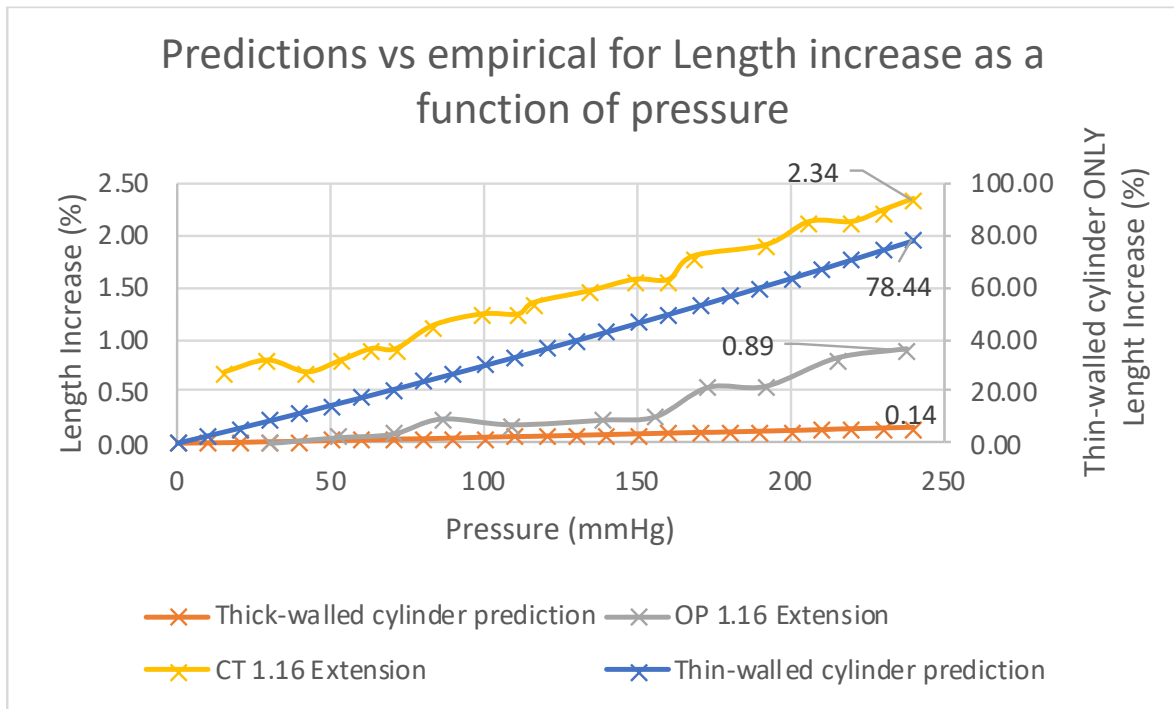


Figure 29: Comparison of prediction and empirical length increase as a function of pressure. Showing both methods of measurements fit better the theoretical data for thin walled cylinders.

Limitations of results

The most significant factors that limit the accuracy of the above results are highlighted below, with ways to mitigate in future investigations.

Table 8: Limitations of results and possible improvements

Method/ Technique	Issues	Improvements
Optical	Assumption that the specimen is perfectly circular (there is no variation in the diameters taken from different angles). Only one diameter measurement (horizontal) was taken as the images were captured from above.	This could be improved with additional cameras at different angles.
	Quality and clarity of some images taken hindered the ability to accurately take measurements. The clarity was affected by water droplets and spray from the specimen leak rate. Additionally, zooming of the image in order to determine the specimen edge, occasionally reduced the image quality. Some images were skipped to prevent large errors being introduced.	This could be improved by the insertion of a latex membrane inside the specimen to prevent transmural leakage similar to the work of Bustos, García-Herrera and Celentano (2016). A higher quality camera could reduce zooming issues.
	Parallax error associated with the image would have introduced error.	Mitigate with more sophisticated camera equipment or calculate parallax angle and adjust.
CT	The predetermined window level 'Bone setting' was used for all images in Osirix Lite. This may have introduced a systematic error across all measurements if the image does not represent the true dimensions.	Attempt to find the most accurate setting by entering the parameter manually.
	The centre of the specimen was determined by eye when taking diameter measurements on different axes.	More accurate predictions of the centre of the circle. This can be calculated with sophisticated software such as ilastik (segmentation, 3D reconstruction) that predicts the centre of mass.
CT and OP	Ill-defined edges affected the accuracy of the length and diameter dimensions.	Use software such as MATLAB to analyse images for longitudinal and circumferential measurements (Madhavan et al., 2012). Alternatively, a CCD (charge-coupled device) Camera was used by Sommer et al. (2018) to measure gauge marking displacement.
Predictions	The predictions are for thick and thin walled cylinder models. These models are normally used for linear elastic materials such as metal with small deformations in rigid pipes.	Use real experimental data to build theoretical models appropriate for finite strain theory such as a hyperelastic constitutive model.
Material Properties	Standard procedure is to use a 'dumbbell' shaped specimen. The entire tubular specimen was used and a change in diameter was measured.	Adhere to standard procedure.
	Errors may have been introduced when measuring original dimensions of the specimens using Image-J. The measurement of the lateral dimensions introduced error due to the specimen being deformed when measured.	This could be alleviated with an extensometer for the lateral measurements as well as the axial.
Rig (See Section 3.4.1)	Chosen specimen doesn't behave like an artery in some tests.	Use a material that is a better representative of an artery.

Discussion of results

Experimental - CT Method

Figure 19 shows how the mean diameter and length vary as internal pressure increases. Diameters 1 and 3 show almost identical deformation changes as expected for the normal sections of the specimen. This suggests that any errors that might be introduced during imaging and measuring (see Section 5) are either evened out with averaging, or systematic, and therefore can be confident that any differences detected between different regions represent true differences in the geometry of the specimen. Diameter 2 on average, increased 6.4% more than that of location 1 and 3. At the lowest pressure of 15mmHg, Diameter 2 has a difference of 7.6% compared to Diameter 1. This demonstrates how much the sutures deform the normal geometry of the specimen even at low pressures. The data also displays the accuracy of the method; smooth curves without deviation are expected to be seen, similar to the predictions (Figure 28 & Figure 29) with a significantly smoother curve than the Optical method (Figure 23). The averaging of 4 diameters is expected to minimise the error introduced during the measurements and therefore increase the likelihood that the measurement is closest to the true value. However, taking diameters without a defined centre likely introduced error as the measurements were not true diameters.

The length increased by a maximum of 2.3% at 240mmHg. The trendline was added in order to extrapolate the data to a pressure of 0mmHg, at which there was an approximate length increase of 0.43%. This suggests a random error was most likely introduced from the ill-defined edges of the Herbie clips when measuring length.

The standard deviation (Figure 20) was calculated for the four values taken for diameters at each pressure for the locations in the CT method. For a perfect circle, a standard deviation of 0 would be expected as all diameters are identical. For all locations the standard deviation decreases as pressure increases due to the specimen becoming more circular.

Whilst the higher pressures of Diameter 2 show a similar standard deviation compared to Diameters 1 and 3, the lower pressures are significantly higher. The variation in diameters at a lower pressure for Diameter 2 represent the distortions to the specimen due to the tension in the sutures of the anastomosis. As the pressure increases, it is enough to overcome the tension in the sutures and gradually make the specimen cross-section more circular as can be seen in Table 6 and Table 7, showing cross-sectional images and 3D volume renders respectively of the specimen from the CT scan.

Approximately 192mmHg is sufficient pressure to reduce the distortion caused by the sutures, thus reducing the St. dev to values similar to Diameters 1 & 3 and making the cross-section more circular. This can be seen on the graph and in the images. It is worth noting that for the highest pressures, the standard deviation is 0.06, 0.07 and 0.05mm for Diameters 1, 2 and 3 respectively. Significantly lower standard deviations show a quasi-circular cross section and although some variation is likely to be random error due to operator measurements, even at 240mmHg (Table 6) the cross-section is slightly elliptical.

Figure 21 shows the four diameter measurements taken during the CT method at Location 1 for each cross section. The horizontal measurement shows lower diameters than the vertical and +45° diameter measurements due to the elliptical shape of the specimen cross-section. It is assumed that only taking the horizontal measurement in the optical method will also be lower demonstrating the superiority of the CT method. It allows an average to be taken to determine a mean diameter of the specimen. The mean diameter in the CT method is a closer prediction to the true value of the specimen and aligns with the predictions more than the OP method (Figure 28).

Figure 22 shows how cross-sectional area increases as pressure increases. This method of analysing the geometry change is assumed to be 'truer' than the mean diameter measurements as any distortions to the shape are included in the measurement. Area results in location 1 and 3 are almost identical and highlight the accuracy of the method as these regions are expected to deform similarly. Figure 19 & Figure 22 show very similar traces and give confidence of the accuracy of the CT methods.

Experimental - Optical Method

Figure 23, in general, the geometry increased with pressure increase. Similar to the results of CT, diameter increase is higher for Location 2 due to the sutures and diameters 1 and 3 follow a similar path. The similarity for diameters 1 and 3 suggests that despite this technique being more manual and measuring along only one axis (horizontal), the values obtained for different regions of the tube can be compared as any errors are consistent and evened out by averaging, thus giving very similar traces for regions 1 and 3.

Whilst diameters 1 and 3 and length show relatively smooth curves, diameter 2 shows more deviation from the smooth curve expected. This may be associated with limitations such as image quality at diameter 2 affected by water droplets. This meant defining the specimen edge was difficult and introduced errors, such as the data label on the graph of 8.91%. In the future, additional repetitions of this experiment and improvements in leakage (See section 5) should be used to reassess this result.

For Figure 19, Figure 22 & Figure 23, the smooth curve represents a fairly constant distensibility. The distensibility does not decrease with pressure thus, a J-curve relationship (Section 2.3) is not displayed, as expected for an elastomeric material. Diameter 2 (Figure 23) does appear to change gradient at higher pressures, however this is likely to be inaccuracies introduced by the OP method as it was not observed in the CT method.

Figure 24 indicates higher percentage increase in diameter for higher pretension values at Location 2. This is similar when comparing the length extensions at different pretensions Figure 25, clearly showing a higher length change for a pretension of 1.25 compared to 1.05, the distinction between 1.05 and 1.16 however was less clear. This increase in axial length change as the pretension is increased contrasts with the work of Sommer et al. (2018) and Bustos, García-Herrera and Celentano (2016). In these studies, extension-inflation tests were conducted on human arteries and Dacron Grafts respectively. However, both studies concluded that circumferential stretch decreases as axial pretension increases, the opposite to

the results of this investigation. Kang (2008) also experienced stiffening of vessels when axial weight increased. However, extension-inflation experiments on elastomeric balloons Mao et al. (2014) showed that the pressure required to inflate the balloon to a specified volume is lower for higher pre-stretches, therefore softening the balloon with increased pre-stretch. These differences between results arise from the different specimens used. As discussed in Section 2.3, when stretched out the collagen in arteries inhibits deformation. The results of this investigation are similar to the results of Mao et al. (2014) in which an isotropic elastomer is used. Katzensteiner (2011) also found that oesophagus samples experienced softening in the circumferential direction for prestretches up to 30% but for higher levels of prestretch, the samples stiffened. Therefore, it could be possible, for this investigation, that the prestretch has not reached the limit at which the material stiffens. Nonetheless, under physiological conditions, the elastomeric specimen behaves differently to human arteries and grafts with respect to pretension and this should be considered if using this system to model anastomosed blood vessels.

In Figure 25, pretensions for 1.05 and 1.16 appear to have little effect on length increases as a function of pressure. It is possible that this is due to problems with image clarity and the accuracy of the measuring technique. It is also assumed that no pretension weight is lost due to the stretch in the fishing wire or friction on the pulley. The small weight difference between pretension 1.05 and 1.16 may have been too little to see a change in results. This result should be reinvestigated in future studies.

Comparisons

Because the OP method did not rely on access to the CT scanner, a number of different measurements/experiments using this technique were conducted. Despite some issues with measurement accuracy, particularly around region 2, similar trends were observed in the data comparing the OP to the CT data. Therefore, it's believed that comparisons between measurements obtained with the OP protocols are viable (see for example, the similarity in the traces between regions 1 and 3 on Figure 23 showing consistency of the measurements).

Figure 26 & Figure 27 show a positive correlation of how geometry increases as a function of pressure.

As expected, diameters 2 (anastomosis) data is also higher in geometry increase than the Diameter 1 due to the sutures. For the maximum pressures of 240 and 238mmHg for CT and OP methods respectively, there is a 2.2% difference between the increases at diameter 2. The two techniques show similar trends, but precise values and percentage increases are not the same. When comparing the relative effects within experiments however, they are similar. A percentage difference for diameter 1 for the highest pressures show approximately 4.2% difference in diameter increase. Lengths at maximum pressure also display a 1.45% increase difference between the two methods (Figure 27).

The differences in data between the methods may arise from the introduction of different errors in the two techniques. In particular, in the OP method, only one diameter is taken (horizontal), which is problematic if the specimen is not perfectly circular. As discussed above, even at high pressures, the specimen is never

perfectly circular. Thus, taking just one diameter measurement in the optical method does not provide an accurate value for the diameter of the specimen. It has also been highlighted that the horizontal measurement was potentially the lowest of the diameter values, compounding the problem of measuring only the horizontal diameter. For the differences in length, the image clarity made measurements difficult when zooming in on the Herbie clips. Precisely determining the centre of the tube for taking the length measurements was also subject to human error and would have varied between methods. A systematic error was also introduced into the CT method when applying the 'Bone setting' to the images, potentially affecting the accuracy throughout the experiment. However, overall, because the bone setting introduced error is likely to be systematic, the CT results are favoured as more accurate.

Figure 28 shows that the empirical data for increase at diameter 1 is generally lower than the predicted data. This graph compares the un-anastomosed part of the specimen experimentally as it is expected that the anastomosed region has a comparatively higher diameter increase. As aforementioned, it is expected that the OP and CT methods should be showing similar deformations but due to the discussions above, particularly the fact that measurements were made horizontally, the axis showing the least deformation, the OP trace is lower than the CT trace. The CT method measuring diameter appears to align with the predictions for thin-walled cylinder towards the higher-pressure values of the experiment. The condition for thin-walled cylinder theory is that "the ratio of radius r to wall thickness t is greater than 10" (Ibrahim, Ryu and Saidpour, 2015) and with average values of $r = 3.56$ and $t = 0.39$ the ratio equates to 9.13. Therefore, the expectation was that the empirical data would align more closely with the thick-walled predictions, however the shape of the smooth curve is still very close to both predictions.

A range of diameters were also derived from the cross-sectional area measurements of the specimen and compared with predictions, showing the highest diameter increase. This may not be appropriate however as the specimen is not perfectly circular and therefore the diameter derived is not true.

Figure 29 displays a large difference between experimental values and predicted values for length increase, but as above appears to align more closely with thin walled cylinder predictions.

It may be that the theoretical predictions are not an appropriate model to use against this empirical data. The governing equations are designed for infinitesimal strain when the specimen is experiencing finite strain. Poisson's ratio is also modelled as a constant when it should be varying with deformation. Nor do the predictions consider pretension, as discussed for Figure 24 increased pretension increases diameter and thus applying pretension to the predictions would result in a higher percentage difference between empirical and predicted values.

Conclusions

The aim if the investigation was to determine how geometry varies with pressure for a synthetic representation of an artery with an anastomosis and how experimental data compares with predicted values. A rig that applies internal pressure and pretension to an anastomosed specimen was successfully designed and built with

simplicity and financial considerations in mind. The rig and two methods were successfully used to analyse the geometric changes of the specimen whilst under internal pressure and pretension. Some errors were introduced, however both methods were deemed to be valid, especially with the improvements discussed.

In general, the specimen geometry experienced a smooth increase in diameter and length as pressure was increased. Empirical data was compared with theoretical predictions. The CT method (diameter) appeared to align with Thin-walled cylinder predictions, however the predictive models used may not be appropriate when considering a non-linearly elastic material. Optical results were lower when compared to the CT method and predictions. It is likely that this is due to current method limitations, however there is scope for this to be improved in future studies.

A range of pretensions was also applied to the specimen and appeared to 'soften' the material, increasing the circumference and length whilst under pressure for higher pretensions. As this contradicts existing literature when considering arterial deformation, this highlights the need to use a material with closer mechanical properties to an artery to truly understand how it will behave. The CT method demonstrated that the ability to take a cross-section of the specimen allowed more accurate measurements to be taken for the diameter and areal deformation in comparison to the Optical method. The standard deviation between diameter measurements of a cross-section also highlighted how internal pressure overcame the tension in the sutures and made the specimen cross-section more circular. The added benefit of the CT scanner is that the above point can be supported by the images taken, clearly seeing less deformation at higher pressures.

This work has been an important step in understanding how the anastomosed region differs to the rest of the artery. In comparison to existing literature, this study has given an insight into the internal shape of the specimen at the anastomosed region and how it changes over a physiological pressure range.

Future work

Address limitations:

- Accurate determination of material properties – addition of lateral extensometer for tensile test.
- Additionally, use a Poisson's Function and Non-linear stretch moduli function (Hyperelastic models) for material properties that vary with strain (Mihai and Goriely, 2017).
- Improve Optical Imaging technique with addition of cameras at different angles.
- Improve CT technique with use of Software for determining centre of specimen.
- Conduct deeper analysis of how geometry changes with respect to the area and volume (CT method.)

Build upon findings:

- Analyse how specimen wall changes geometry (CT).

- Consider cyclically preconditioning specimens before use (Sommer et al., 2018).
- Consider that extended use of the specimen may result in hardening or brittle effects.
- Consider how the unpredictable behaviour of a non-Newtonian fluid (blood) could affect the results of this investigation (Sarkar, Salacinski, Hamilton and Seifalian, 2006).
- Consider how different Suture techniques, knot strength and tension affect the results of this investigation (Roussis et al., 2015).

Due to time constraints it was not possible to make use of the 3D reconstructed models of the internal geometry of the specimens from the CT scans. However, this technique is feasible. Further work could include:

- CAD conversion for analysis of volume and mass.
- Creating a computer model and simulation for deformation of specimen.

Acknowledgements

Throughout the entirety of this research I have received a great deal of support and assistance. Firstly, I am extremely grateful to my supervisor, Mr Adam Kyte, whose consistent guidance and support, vast array of knowledge and patience was invaluable. Secondly, Dr Jahir Rizvi, for his crucial feedback during the early stages of the paper.

I would like to acknowledge Dr Carl Roobottom, Colin Stuckey and Derriford Computed Tomography Unit for their experience and access to the facilities at Derriford Hospital, without which the scope of the research may have been different. I would also like to thank Sandra Shurey, for her skill and expertise in preparing numerous specimens. Mr Terry Richards for his assistance and experience in the University laboratories. In addition, I would like to thank Sara for her sympathetic ear, and all the people whose assistance was a milestone in the completion of this paper.

Reference List

Burton, A., 1954. Relation of Structure to Function of the Tissues of the Wall of Blood Vessels. *Physiological Reviews*, 34(4), pp.619-642.

Bustos, C., García–Herrera, C. and Celentano, D. (2016). Modelling and simulation of the mechanical response of a Dacron graft in the pressurization test and an end-to-end anastomosis. *Journal of the Mechanical Behaviour of Biomedical Materials*, 61, pp.36-44.

Chen, M., Chen, A., Si, X., Ji, M. and Zheng, D., 2017. Peripheral arterial volume distensibility changes with applied external pressure: significant difference between arteries with different compliance. *Scientific Reports*, 7(1).

Goriely, A., Destrade, M. and Ben Amar, M., 2006. Instabilities in elastomers and in soft tissues. *The Quarterly Journal of Mechanics and Applied Mathematics*, 59(4), pp.615-630.

Hearn, E. (1997). *Mechanics of Materials: The mechanics of elastic and plastic deformation of solids and structural materials*. Oxford: Butterworth-Heinemann, pp.198-222.

Hulse, R. and Cain, J. (2001). *Structural mechanics*. 2nd ed. Basingstoke: Palgrave, pp.155-156.

Ibrahim, A., Ryu, Y. and Saidpour, M. (2015). Stress Analysis of Thin-Walled Pressure Vessels. *Modern Mechanical Engineering*, 05(01), pp.1-9.

Kang, T., 2008. Mechanical behavior of arteries under inflation and extension. *Journal of Mechanical Science and Technology*, 22(4), pp.621-627.

Katzensteiner, A., 2011. Uniaxial Tensile, Rupture and Extension-Inflation tests on ovine esophagi. Masters. Graz University of Technology.

Madhavan, K., Elliott, W., Bonani, W., Monnet, E. and Tan, W. (2012). Mechanical and biocompatible characterizations of a readily available multilayer vascular graft. *Journal of Biomedical Materials Research Part B: Applied Biomaterials*, 101B(4), pp.506-519.

Mao, G., Li, T., Zou, Z., Qu, S. and Shi, M., 2014. Prestretch effect on snap-through instability of short-length tubular elastomeric balloons under inflation. *International Journal of Solids and Structures*, 51(11-12), pp.2109-2115.

Matsuda, T. and He, H., 2002. Newly Designed Compliant Hierarchic Hybrid Vascular Grafts Wrapped with a Microprocessed Elastomeric Film—I: Fabrication Procedure and Compliance Matching. *Cell Transplantation*, 11(1), pp.67-74.

Melly, L., Torregrossa, G., Lee, T., Jansens, J. and Puskas, J., 2018. Fifty years of coronary artery bypass grafting. *Journal of Thoracic Disease*, 10(3), pp.1960-1967.

Mihai, L. and Goriely, A., 2017. How to characterize a nonlinear elastic material? A review on nonlinear constitutive parameters in isotropic finite elasticity. *Proceedings of the Royal Society A: Mathematical, Physical and Engineering Sciences*, 473(2207), p.20170607.

Mihai, L., Chin, L., Janmey, P. and Goriely, A., 2015. A comparison of hyperelastic constitutive models applicable to brain and fat tissues. *Journal of The Royal Society Interface*, 12(110), p.20150486.

Mott, P., Dorgan, J. and Roland, C., 2008. The bulk modulus and Poisson's ratio of "incompressible" materials. *Journal of Sound and Vibration*, 312(4-5), pp.572-575.

Perktold, K., Leuprecht, A., Prosi, M., Berk, T., Czerny, M., Trubel, W. and Schima, H., 2002. Fluid Dynamics, Wall Mechanics, and Oxygen Transfer in Peripheral Bypass Anastomoses. *Annals of Biomedical Engineering*, 30(4), pp.447-460.

Philpot, T., 2014. *Mechanics Of Materials*. 3rd ed. Hoboken, NJ: John Wiley, p.59.

Roeder, R., Wolfe, J., Lianakis, N., Hinson, T., Geddes, L. and Obermiller, J., 1999. Compliance, elastic modulus, and burst pressure of small-intestine submucosa (SIS), small-diameter vascular grafts. *Journal of Biomedical Materials Research*, 47(1), pp.65-70.

Roussis, P., Giannakopoulos, A., Charalambous, H., Demetriou, D. and Georghiou, G., 2015. Dynamic behavior of suture-anastomosed arteries and implications to vascular surgery operations. *BioMedical Engineering OnLine*, 14(1), p.1.

Sanborn, B. and Song, B., 2019. Poisson's ratio of a hyperelastic foam under quasi-static and dynamic loading. *International Journal of Impact Engineering*, 123, pp.48-55.

Sarkar, S., Salacinski, H., Hamilton, G. and Seifalian, A., 2006. The Mechanical Properties of Infrainguinal Vascular Bypass Grafts: Their Role in Influencing Patency. *European Journal of Vascular and Endovascular Surgery*, 31(6), pp.627-636.

Sasso, M., Palmieri, G., Chiappini, G. and Amodio, D., 2008. Characterization of hyperelastic rubber-like materials by biaxial and uniaxial stretching tests based on optical methods. *Polymer Testing*, 27(8), pp.995-1004.

Schiller, N., Franz, T., Weerasekara, N., Zilla, P. and Reddy, B., 2010. A simple fluid–structure coupling algorithm for the study of the anastomotic mechanics of vascular grafts. *Computer Methods in Biomechanics and Biomedical Engineering*, 13(6), pp.773-781.

Sommer, G., Benedikt, C., Niestrawska, J., Hohenberger, G., Viertler, C., Regitnig, P., Cohnert, T. and Holzapfel, G. (2018). Mechanical response of human subclavian and iliac arteries to extension, inflation and torsion. *Acta Biomaterialia*, 75, pp.235-252.

Sonoda, H., Urayama, S., Takamizawa, K., Nakayama, Y., Uyama, C., Yasui, H. and Matsuda, T. (2002). Compliant design of artificial graft: Compliance determination by new digital X-ray imaging system-based method. *Journal of Biomedical Materials Research*, 60(1), pp.191-195.

Southampton.ac.uk. 2020. *Prices | M-VIS: Multidisciplinary, Multiscale, Microtomographic Volume Imaging | University Of Southampton*. [online] Available at: <<https://www.southampton.ac.uk/muvis/access/prices.page>> [Accessed 13 May 2020].

Upstate Medical University, 2020. *Displaying Images (Window/Level Settings) | Radiology | SUNY Upstate Medical University*. [online] Available at: <<https://www.upstate.edu/radiology/education/rsna/intro/display.php>> [Accessed 22 April 2020].

Zhalmuratova, D. and Chung, H., 2020. Reinforced Gels and Elastomers for Biomedical and Soft Robotics Applications. *ACS Applied Polymer Materials*, 2(3), pp.1073-1091.

Zilla, P., Bezuidenhout, D. and Human, P., 2007. Prosthetic vascular grafts: Wrong models, wrong questions and no healing. *Biomaterials*, 28(34), pp.5009-5027.